# Luminescent Carbon Nanodots: Emergent Nanolights

*Sheila N. Baker* and Gary A. Baker**

*In memory of Robert D. Fugate*

*Angewandte*
*Chemie*
International Edition
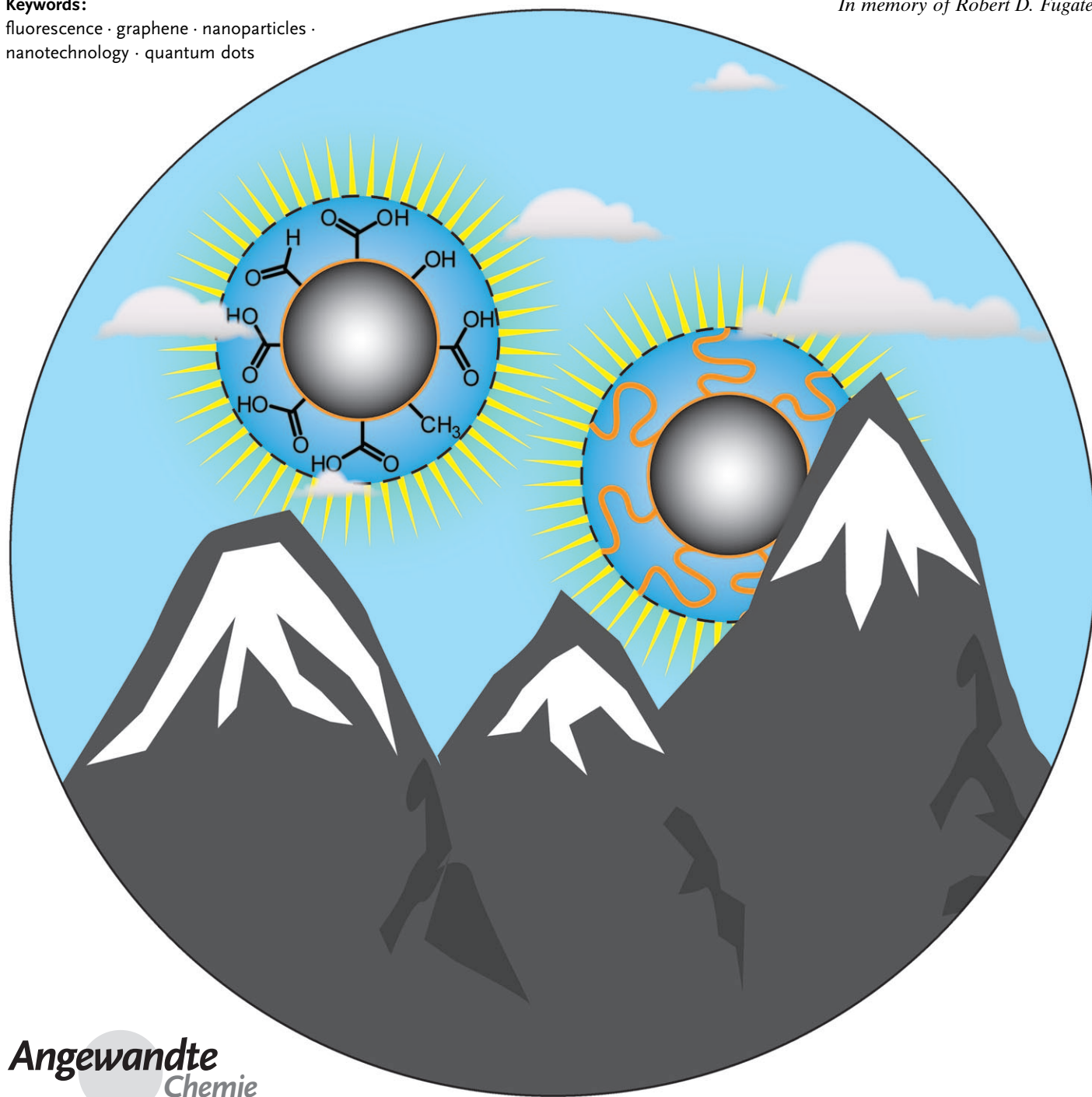
**S**imilar to its popular older cousins the fullerene, the carbon nano-
tube, and graphene, the latest form of nanocarbon, the carbon
nanodot, is inspiring intensive research efforts in its own right. These
surface-passivated carbonaceous quantum dots, so-called C-dots,
combine several favorable attributes of traditional semiconductor-
based quantum dots (namely, size- and wavelength-dependent lumi-
nescence emission, resistance to photobleaching, ease of bioconju-
gation) without incurring the burden of intrinsic toxicity or elemental
scarcity and without the need for stringent, intricate, tedious, costly, or
inefficient preparation steps. C-dots can be produced inexpensively
and on a large scale (frequently using a one-step pathway and
potentially from biomass waste-derived sources) by many approaches,
ranging from simple candle burning to in situ dehydration reactions to
laser ablation methods. In this Review, we summarize recent advances
in the synthesis and characterization of C-dots. We also speculate on
their future and discuss potential developments for their use in energy
conversion/storage, bioimaging, drug delivery, sensors, diagnostics,
and composites.

## From the Contents

## 1. Introduction

Carbon nanodots (C-dots) constitute a fascinating class of recently discovered nanocarbons that comprise discrete, quasispherical nanoparticles with sizes below 10 nm.[1–23] Typically displaying size and excitation wavelength ($\lambda_{ex}$) dependent photoluminescence (PL) behavior, C-dots are attracting considerable attention as nascent quantum dots, particularly for applications in which the size, cost, and biocompatibility of the label are critical. Advances in this area are appearing frequently, with a number of significant break-throughs taking place within the last couple years. Several of the seminal advances made to date are illustrated in Figure 1.

Typically, C-dots contain many carboxylic acid moieties at their surface, thus imparting them with excellent water solubility and the suitability for subsequent functionalization with various organic, polymeric, inorganic, or biological species (Figure 2). Their well-defined, nearly isotropic shapes together with their ultrafine dimensions, tunable surface functionalities, and the sheer variety of simple, fast, and cheap synthetic routes available provide an encouraging technological platform for C-dot emitters as alternatives to other nanocarbons (fullerenes, nanodiamonds, carbon nano-tubes) in a host of applications. Most notable, however, is their potential as replacements for toxic metal-based quan-tum dots (QDs) currently in use. As a consequence of the health concerns and the known environmental and biological hazards of QDs, C-dots are at the center of significant research efforts to develop low-toxicity, eco-friendly alter-natives that have the desirable performance characteristics of QDs. C-dots have already demonstrated their viability in a variety of applications since they display PL properties reminiscent of those of QDs[24–26] and surface-oxidized Si nanocrystals.[27–29]

Ironically, C-dots were discovered serendipitously by researchers purifying single-walled carbon nanotubes (SWCNTs) fabricated by arc-discharge methods.[1] When processing a suspension of these SWCNTs by gel electro-phoresis, much to these researchers' surprise, the suspension separated into three distinct classes of nanomaterials, includ-ing a fast-moving band of highly luminescent material. They further found that this carbonaceous material could be fractionated into a number of components with size-depen-dent fluorescent properties. While certainly not the SWCNTs they were looking for, the researchers went on to analyze the basic properties of this then-unknown fluorescent nanomate-rial, with the astute assertion that they "promise to be interesting nanomaterials in their own right".[1] Since their initial discovery, these materials have come to be known as carbon dots or carbon nanodots, and have been studied and fabricated by numerous research groups hoping to glean a better understanding into the origins of their photophysical behavior, achieve better synthetic routes, and develop novel applications for these emergent nanomaterials.
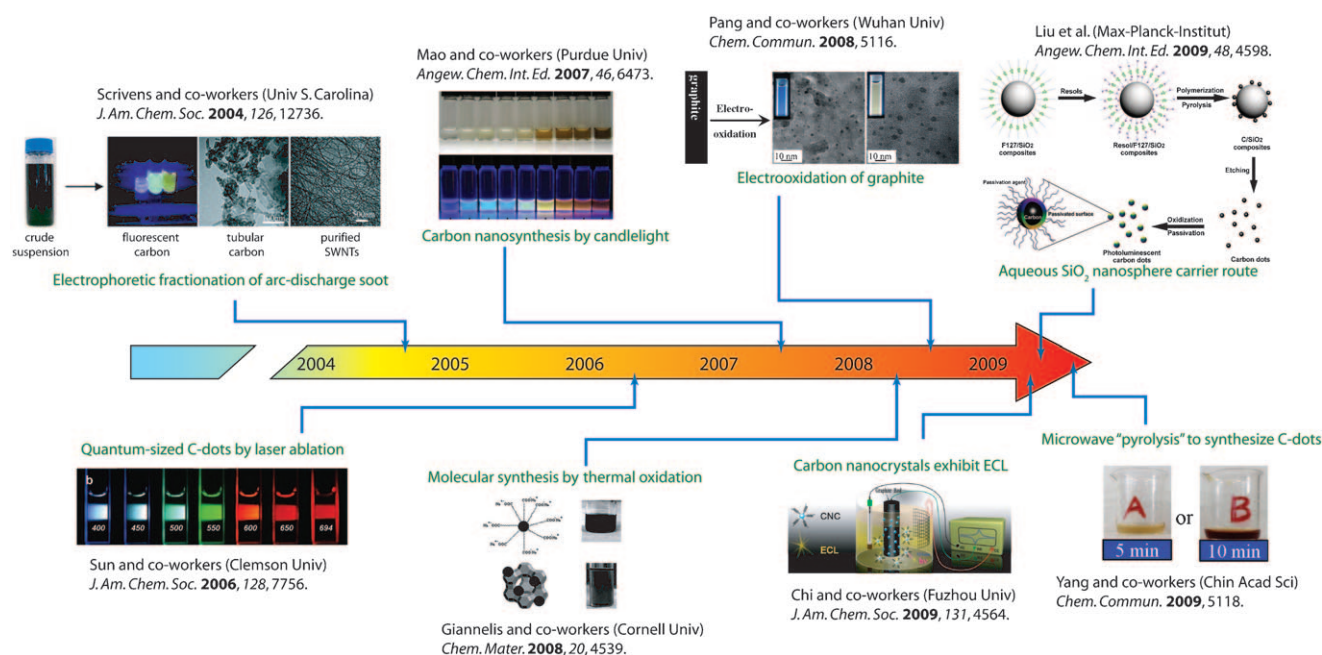
Another carbon-based nanomaterial similar in size and surface functionality to the C-dot is the nanodiamond, which has been recently reviewed.[30–33] For clarification purposes, one should take care in distinguishing these two types of
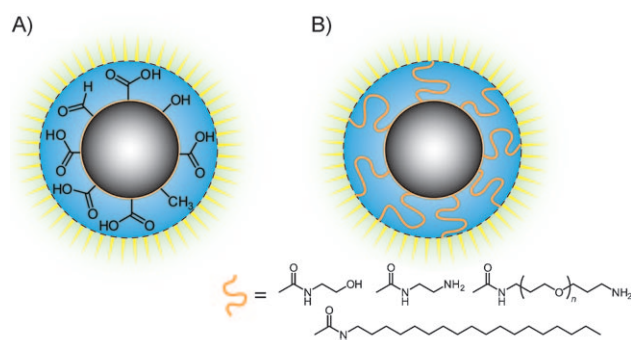
[*] Dr. S. N. Baker, Dr. G. A. Baker
    Oak Ridge National Laboratory
    1 Bethel Valley Road, Oak Ridge, TN 37831-6201 (USA)
    Fax: (+1) 865-574-6080
    E-mail: sb3@ornl.gov
          bakerga1@ornl.gov

**Figure 1.** Timeline showing recent activity regarding C-dots in the literature. Reproduced from Refs. [1, 2, 7, 9, 12, 17, 18, 20].



**Figure 2.** Depiction of C-dots A) after surface oxidative treatment and B) after functionalization with surface-passivation reagents.

carbon-based nanomaterials. Nanodiamonds are typically made from milling microdiamonds, chemical vapor deposition (CVD), shockwave, or detonation processes. They generally consist of about 98% carbon with residual hydrogen, oxygen, and nitrogen, possess a $sp^3$ hybridized core, and have small amounts of graphitic carbon on the surface. Unlike nanodiamonds, C-dots have greater $sp^2$ character, which is symbolic of nanocrystalline graphite (in this way, they might rightfully be considered close relatives to the graphene quantum dot, discussed in Section 5), and contain lower amounts of carbon with higher oxygen contents. Sometimes, because of their high oxygen content, these materials have also been referred to as carbogenic nanodots.[2,3,23] While C-dots show spectrally broad (unstructured) PL emission with strong $\lambda_{ex}$ dependency, fluorescent nanodiamonds emit from point defects, particularly the negatively charged nitrogen vacancy site, which absorbs strongly at 569 nm and emits near 700 nm. Although the origins of PL are not yet entirely understood in C-dots, there is mounting evidence that emission arises from the radiative recombination of excitons located at surface energy traps which may or may not require passivation by organic molecules to occur.

Section 2 of this Review describes the various synthetic routes used to produce C-dots (Table S1 in the Supporting Information summarizes the general properties of C-dots made by the different fabrication approaches). Section 3 considers their prominent physicochemical and optical prop-

Sheila Baker was born in the US in 1974. She obtained her BS in Chemistry in 1997 at Georgia Southern University, , and then her PhD in 2002 (F. V. Bright) at the University at Buffalo. After a postdoctoral stay at Los Alamos National Laboratory (T. M. McCleskey) and a one-year stint at a biotech start-up, she joined Oak Ridge National Laboratory in 2008. Her primary research interests include sub- and supercritical fluids, designer ionic liquids, magnetic and morphologically unique nanostructures, and materials for next-generation photovoltaics, batteries, and supercapacitors.

Gary Baker studied chemistry at SUNY Oswego followed by the University at Buffalo where he earned a PhD in 2001 in the group of professor Frank V. Bright. After completing Director's and Frederick Reines Postdoctoral Fellowships at Los Alamos National Laboratory, he joined the research staff at Oak Ridge National Laboratory as a Wigner Fellow in 2005. His research interests focus on solar cells, ionic liquids, and smart nanomaterials. He recently received a Presidential Early Career Award for Scientists and Engineers (PECASE) in 2008.

erties, with some discussion of preliminary toxicological evaluation. Their application as labels for bioimaging is the topic of Section 4. Section 5 provides an account of the recent observation of PL in graphene-based materials. It is our aim that the synthesis of this knowledge will offer valuable insight but, moreover, we hope to inspire research into the origins of the unique properties of this emergent class of nanocarbons and to encourage their exploration in a multitude of exciting areas, ranging from medical diagnostics to catalysis and photovoltaics.

## 2. Synthetic Methods

Approaches for synthesizing C-dots can be generally classified into two main groups: top-down and bottom-up methods. Top-down methods consist of arc discharge,[1] laser ablation,[4–6,11,12,14–16] and electrochemical oxidation,[8,17–19] where the C-dots are formed or "broken off" from a larger carbon structure. Bottom-up approaches consist, for example, of combustion/thermal,[2,3,7,10,13] supported synthetic,[2,9] or microwave methods[20] during which the C-dots are formed from molecular precursors. Typically, their surfaces are oxidized by nitric acid ($HNO_3$) and further purified by using centrifugation, dialysis, electrophoresis, or another separation technique.

### 2.1. Top-Down Approaches
#### 2.1.1. Arc-Discharge Methods

While purifying SWCNTs derived from arc-discharge soot, Xu et al. discovered they had also isolated an unknown fluorescent carbon nanomaterial.[1] They started by first oxidizing arc soot with 3.3 N $HNO_3$ to introduce carboxyl functional groups, which improved the hydrophilicity of the material. The sediment was then extracted with an NaOH solution (pH 8.4), which resulted in a stable black suspension. This suspension was separated by gel electrophoresis into SWCNTs, short tubular carbons, and what can now referred to as C-dots. The C-dots were separated into three electrophoretic bands which upon excitation at 366 nm emitted green-blue, yellow, and orange in order of their elution and increasing size, as determined by partitioning with different nominal molecular weight (MW) cut-off Centricon filtration devices. FTIR analysis revealed the presence of carboxyl functionalities and, most importantly, the absence of characteristic C−H out of plane bending modes of polyaromatic hydrocarbons (PAHs), thus indicating that the origin of the PL was not derived from PAH sources. Elemental analysis revealed the C-dots contained 53.9% C, 2.6% H, 1.2% N, and 40.3% O.

#### 2.1.2. Laser-Ablation Methods

More recently, C-dots have been purposefully produced by Sun and co-workers by laser ablation.[4,6,11,12,14–16] These researchers prepared a carbon target by hot-pressing a mixture of graphite powder and cement, followed by stepwise

baking, curing, and annealing under an argon flow.[12] A Q-switched Nd:YAG laser (1064 nm, 10 Hz) was then used to ablate the carbon target in a flow of argon gas carrying water vapor at 900°C and 75 kPa. The sample was then heated at reflux in 2.6 M $HNO_3$ for up to 12 h to produce C-dots ranging from 3 to 10 nm in size. At this point, the C-dots were surface passivated by polymeric agents such as diamine-terminated poly(ethylene glycol) ($PEG_{1500N}$)[12] or poly(propionyl-ethylenimine-*co*-ethylenimine) (PPEI-EI, with an EI fraction of ca. 20%)[4] and then purified by dialysis against water, followed by a centrifugation step to yield purified C-dots in the supernatant liquid.[11] A slightly modified version of this procedure using ^{13}C powder and more rigorous control resulted in ^{13}C-enriched C-dots 4–5 nm in diameter which exhibited a PL quantum yield (QY) of up to 20% with excitation at 440 nm.[16]

A single-step procedure that integrated synthesis and passivation was reported by Hu et al. (Scheme 1).[6] In this approach, a pulsed Nd:YAG laser was used to irradiate
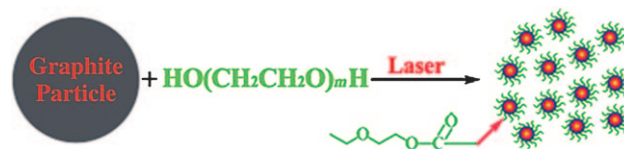


**Scheme 1.** One-step synthesis of C-dots in $PEG_{200N}$ solvent. Reproduced from Ref. [6] with permission.

graphite or carbon black dispersed in diamine hydrate, diethanolamine, or $PEG_{200N}$ for 2 h while under ultrasonication to aid in particle dispersal. After laser irradiation, centrifugation was used to precipitate residual carbon powder fragments while C-dots remained suspended in the supernatant. These C-dots averaged 3 nm in size, with lattice spacings varying from 0.20–0.23 nm, similar to that of diamond. However, we note that these lattice spacings may also reflect the (100) facet of graphite, as further discussed in Section 3. Similar C-dots were obtained by laser irradiation of carbon powders in water followed by oxidation and passivation with a boiling perchloric acid/$PEG_{200N}$ solution for 72 h.

#### 2.1.3. Electrochemical Synthesis

Electrochemical synthesis of C-dots was first demonstrated by Zhou et al.[19] when they grew multiwalled carbon nanotubes (MWCNTs) formed from scrolled graphene layers on carbon paper by CVD. These nanotubes were designed to serve as the working electrode in an electrochemical cell consisting of a Pt wire counter electrode and a Ag/$AgClO_4$ reference electrode with degassed acetonitrile solution containing 0.1 M tetrabutylammonium perchlorate ($TBA^+ClO_4^-$) as the electrolyte. Cycling the applied potential between −2.0 and +2.0 V at a scan rate of 0.5 V s$^{-1}$ resulted in the solution changing from colorless to yellow to dark brown, which indicated the exfoliation of C-dots from the MWCNTs and their accumulation in solution. The C-dots were recovered by evaporating the acetonitrile, dissolving the remaining solid containing the C-dots in water, and dialyzing to remove any remaining electrolyte salt. The C-dots produced were spher-

ical, had diameters of $(2.8 \pm 0.5)$ nm, had lattice spacings consistent with nanocrystalline graphite (Figure 3), and exhibited $\lambda_{ex}$-dependent PL. The structural evolution of the
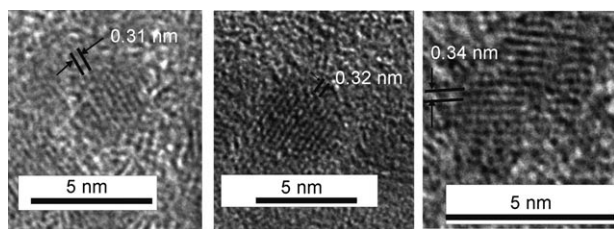


***Figure 3.*** Representative HRTEM images of C-dots. Reproduced from Ref. [19] with permission.

MWCNTs, as monitored by scanning electron microscopy (SEM), revealed that after electrochemical cycling, the MWCNTs had became entangled and swollen with curled features. The authors proposed that the organic $TBA^+$ ions had intercalated into gaps of the MWCNTs during the cycling of the potential, thereby breaking the tubes near these defects to release C-dots. This was further substantiated by experiments using KCl and $KClO_4$ as electrolyte salts, which failed to result in the production of C-dots. No C-dots were formed either when carbon paper without any MWCNTs was used.

Another research group produced C-dots electrochemically by oxidizing a graphitic column electrode at 3 V against a saturated calomel electrode with a Pt wire counter electrode in 0.1 M $NaH_2PO_4$ aqueous solution.[17] The solution underwent a colour change from transparent to dark brown as the oxidation time increased. The solution was then centrifuged to remove any large or agglomerated particles, and the C-dots remaining in the supernatant were size-separated using centrifugal filter devices with MW cutoffs of $< 5$, 5–10, 10–30, and $> 30$ kDa. C-dots recovered from the smaller two MW fractions had diameters of $(1.9 \pm 0.3)$ nm and $(3.2 \pm 0.5)$ nm, respectively. High-resolution transmission electron microscopy (HRTEM) measurements revealed that the C-dots were graphitic in nature, with a lattice spacing of 3.28 Å coincident with the (002) facet of graphite. The PL of these C-dots was size-dependent, with emission maxima of 445 nm and 510 nm for the 1.9 and 3.2 nm dots, respectively.

Chi and co-workers also produced C-dots electrochemically from a graphite rod working electrode, a Pt mesh counter electrode, and a Ag/AgCl reference electrode assembly immersed in pH 7.0 phosphate buffer solution (Scheme 2).[18] When cycling between $-3.0$ and $+3.0$ V, the solution yellowed initially and eventually became dark brown, as other research groups have noted. HRTEM results showed two modalities of spherical C-dots were produced with average sizes of about 20 nm and 2 nm, which were separated using a 10 kDa cutoff membrane.

A variety of carbon-based nanoparticles, including C-dots, were generated by ionic liquid (IL) assisted electrooxidation of graphite using the water-soluble IL 1-butyl-3-methylimidazolium tetrafluoroborate [bmim][$BF_4$] containing up to 90 wt% water as the electrolyte.[8] ILs are salts which melt below 100 °C that are comprised typically of bulky, asymmetric organic cations paired with weakly coordinating, fluorine-
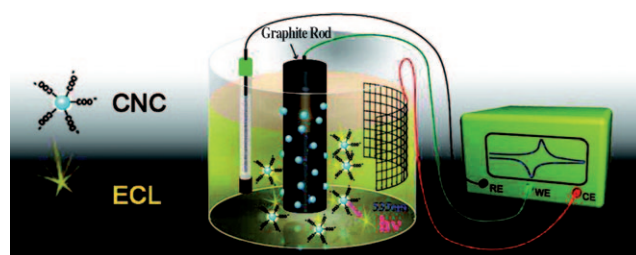


***Scheme 2.*** Electrochemical production of C-dots from a graphite rod which are capable of electrochemiluminescence (ECL). Reproduced from Ref. [18] with permission.

containing anions. The unique properties (nonvolatility, high thermal stability, ionic conductivity, nonflammability, broad liquid range, and wide electrochemical window) have resulted in these designer solvents finding a variety of uses including their utilization as electrolytes in batteries, electrophoresis, fuel cells, and supercapacitors, as well as in solar cell applications.[34] Three distinct time stages were defined during the IL-assisted electrochemical formation of C-dots. In the inductive stage, the solution color darkened and 8–10 nm C-dots were released by oxidation of the graphite anode by $OH\cdot$ and $O\cdot$ radicals. The oxidation occurred initially at graphite edge sites, grain boundaries, or defect sites, which resulted in an opening up of the edge sheets. This facilitated the second stage by providing a path for $BF_4^-$ ions to intercalate into the anode, thereby causing a depolarization and expansion of the graphite anode. The predominant products released in this second stage were fluorescent nanoribbons roughly $10 \times 60$ nm in size that resulted from oxidative cleavage of the expanded sheet. In the third stage, larger expanded sheets peeled off from the anode to form a black slurry in the solution. Both the C-dots and the nanoribbons produced were of graphitic nature, as determined from characteristic lattice spacings measured using HRTEM.

Increasing the water-to-IL ratio resulted in a more-efficient production of C-dots, while decreasing this ratio resulted in a larger fraction of nanoribbons. Changing the IL anion to $Cl^-$ also increased the production of nanoribbons over C-dots. The process progressed in neat IL (their hygroscopic nature means that small amounts of water are invariably present), with the solution evolving to a light yellow to dark brown color and eventually forming a highly viscous solution containing a "bucky gel". C-dots could be isolated from both the gel and supernatant fluid. For relatively low water conditions ($< 10$ wt%), the C-dots obtained were 2–4 nm in diameter, with lattice spacings of 0.33 nm, and were found to be functionalized by the IL.

## 2.2. Bottom-up Approaches
### 2.2.1. Combustion/Thermal Routes

Soot derived from the combustion of unscented candles or natural gas burners forms an elegantly simple source of C-dots.[7,10,13] First presenting this intriguing approach, Mao and co-workers collected soot by placing a piece of aluminium foil

**6730** www.angewandte.org

© 2010 Wiley-VCH Verlag GmbH & Co. KGaA, Weinheim

*Angew. Chem. Int. Ed.* **2010**, *49*, 6726–6744

or a glass plate atop a burning candle. The collected soot was then mixed with 5 m $HNO_3$ and refluxed for 12 h to oxidize particle surfaces. After cooling, the formed C-dots ($<2$ nm) were collected by centrifugation or dialysis and further subjected to polyacrylamide gel electrophoresis (PAGE) fractionation. Similar to the observations of Xu et al.,[1] the C-dot electrophoretic mobilities were correlated with the PL emission color, with faster moving C-dots emitting at shorter wavelengths (Figure 4). The C-dots were found to be roughly
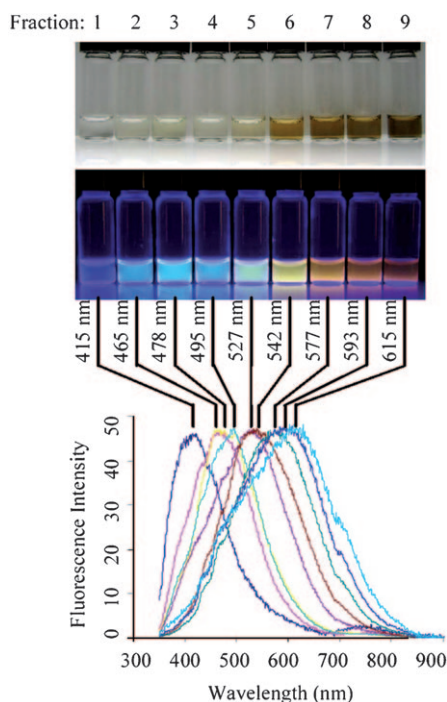


**Figure 4.** Optical characterization of PAGE separated C-dots produced from candle soot. Optical images illuminated under white (top) and UV light (312 nm; center). Bottom: Fluorescence emission spectra ($\lambda_{ex}$ at 315 nm) of the corresponding C-dot solutions. The maximum emission wavelengths are indicated above the spectra. Reproduced from Ref. [7] with permission.

1 nm in height by using AFM, however, no additional measurements were used to further elucidate their size and morphology. From $^{13}$C NMR measurements, three types of carbon signals were observed: external C=C bonds, internal C=C bonds, and C=O bonds. Importantly, no evidence for sp$^3$-hybridized carbon was found. The make-up of the purified C-dots (36.8% C, 5.9% H, 9.6% N, 44.7% O) was vastly different from that of the raw candle soot (91.7% C, 1.8% H, 1.8% N, 4.4% O), with the significantly higher oxygen content due in part to the presence of surface carbonyl groups. The solubility of the C-dots was determined to be about 30 mg mL$^{-1}$ in water, 18 mg mL$^{-1}$ in methanol, 20 mg mL$^{-1}$ in dimethylformamide (DMF), and 41 mg mL$^{-1}$ in dimethylsulfoxide. The PL of the C-dots was both $\lambda_{ex}$- and pH-dependent, with peak emissions in the 415–615 nm range and increased broadening of the bands at longer wavelengths (Figure 4). Interestingly, no external surface passivation agent, as required for other approaches, was needed for PL to occur

by using this approach. This important point is further discussed in Section 3.

This candle-burning approach was also followed by Ray et al. [10] The candle soot was similarly collected and refluxed with 5 m $HNO_3$ for 12 h. It was found that refluxing for under 12 h gave a lower C-dot yield, while refluxing for longer periods resulted in no appreciable gain in yield. The particles suspended in solution were then precipitated by adding acetone and centrifuging at 14 000 rpm for 10 minutes. Size separation was then performed in a water/ethanol/chloroform solvent mixture combined with high-speed, stepwise centrifugation. Supernatant was collected at spinning speeds of 4000, 5000, 6000, and 8000–16 000 rpm, in each case starting with the supernatant collected from the previous step. The supernatant obtained with centrifugation at 8000 rpm, for which precipitate was no longer observed, contained C-dots with particle sizes in the 2–6 nm range. Precipitates at lower centrifugation speeds contained large carbon nanoparticles of 201–350 nm in size. The 2–6 nm C-dots were found to be graphitic in nature, according to lattice spacings in HRTEM images, and exhibited high PL quantum yields in comparison with the larger particles found. XPS compositional analysis, while insensitive to hydrogen, revealed the presence of C, O, and N at 59, 37, and 4 atom%, respectively.

In a further study, Chen and co-workers purified C-dots from the combustion soot of natural gas.[13] By inverting a glass beaker above the flame of a natural gas burner, they were able to collect around 100 mg of soot, which was then refluxed in 5 m $HNO_3$ for 12 h, followed by centrifugation and dialysis to afford purified C-dots of $(4.8 \pm 0.6)$ nm diameter. The as-purified C-dots (no gel electrophoresis was performed in this case) exhibited PL, again without the need for surface passivation, with a $\lambda_{ex}$ maximum of 310 nm and an emission wavelength ($\lambda_{em}$) maximum of 420 nm. No experiments were conducted to determine if the emission characteristics showed a $\lambda_{ex}$ dependence as was noted for other C-dots. HRTEM measurements revealed lattice spacings of 0.208 nm, 0.334 nm, 0.194 nm, and 0.186 nm, which is consistent with the (102), (006), (104), and (105) diffraction planes of sp$^2$ graphitic carbon (Figure 5). $^{13}$C NMR and FTIR measurements also revealed the presence of sp$^2$ carbon and carboxylic/carbonyl moieties, thus leading the authors to conclude that the C-dots most likely consist of a nanocrystalline core featuring graphitic sp$^2$ carbon atoms and a surface functionalized with carboxylic/carbonyl moieties. Interestingly, in contrast to C-dots made from candle combustion, no N (as determined from XPS data) was found to be present in these C-dots.

Giannelis and co-workers used a one-step thermal decomposition of low-temperature-melting molecular precursors to form surface-passivated C-dots that were either hydrophilic or organophilic in nature.[3] This process is highly attractive in that it directly leads to surface-passivated C-dots with precisely engineered surface properties and, by careful selection of the carbon source and surface modifier, better control over the geometry and physical properties of the C-dots is possible. In this study, C-dots were produced by employing two different routes, both yielding monodispersed C-dots with sizes less than 10 nm. In the first route, an
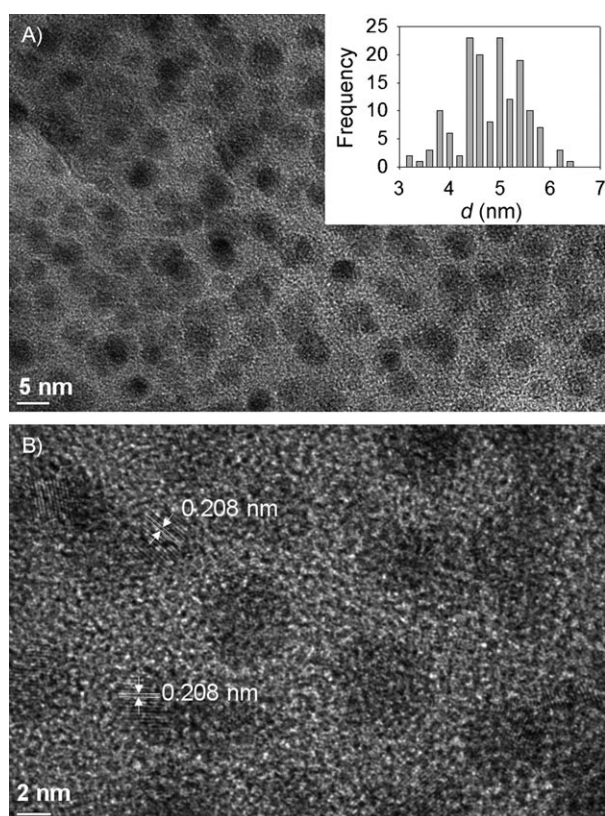
***Figure 5.*** Representative TEM micrographs of C-dots at (a) low and (b) high resolution. Reproduced from Ref. [13] with permission.

ammonium citrate salt served as the molecular precursor, with the citrate providing the carbon source and the ammonium the stabilizer, the nature of which determines the hydrophilicity of the resultant C-dot. Organophilic C-dots were obtained by directly calcining octadecylammonium citrate in air at 300 °C for 2 h, washing with acetone and ethanol, before drying. Hydrophilic particles were obtained by heating diethylene glycolammonium citrate hydrothermally in a teflon-lined stainless steel autoclave at 300 °C for 2 h and washing with acetone. In the second route, 4-aminoantipyrine (4AAP), which acted as the molecular precursor, was calcined in air at 300 °C for 2 h, dissolved in trifluoroethylene, precipitated by the addition of water, and washed several times with ethanol. The first route (citrate salt) provided nearly spherical morphologies of 7 nm C-dots. XRD results showed peaks consistent with highly disordered carbon and densely packed alkyl chains for the organophilic C-dot, with the hydrophilic C-dots adopting a more amorphous structure. 4AAP-derived C-dots were more irregular in shape and were 5–9 nm in size; XRD analysis revealed highly disordered carbon with densely packed phenyl groups. All three types of C-dots displayed the $\lambda_{ex}$-dependent PL emission that is generally characteristic of C-dots.

In a follow-up study, Giannelis and co-workers reported a similar one-step thermal decomposition to C-dots by first protonating the amine group of sodium 11-aminoundecanoate with citric acid followed by heating the compound directly in air at 300 °C for 2 h.[2] The resultant C-dots possessed a total size of 10–20 nm, consisting of a 5–10 nm carbogenic core with a corona made up of a thick ionic shell. An essential feature of this C-dot is the sodium ions ($Na^+$) decorating its outer shell, thus providing an ion-exchange handle for tuning features such as solubility. For example, as-prepared C-dots were water-soluble and precipitated at low pH (ca. 2); however, ion exchange of the $Na^+$ ion with the cetyltrimethylammonium cation resulted in organophilic C-dots that were dispersible in tetrahydrofuran.

### 2.2.2. Supported Routes

Another bottom-up synthetic strategy involves the use of supports on which to grow the C-dots. In this way, the support serves to localize the growth of C-dots, by blocking nanoparticle agglomeration during high-temperature treatment.

One such route was employed by Li and co-workers, who used surfactant-modified silica spheres as supports (Scheme 3).[9] Firstly, composites were prepared by modifying silica spheres with F127, an amphiphilic triblock copolymer.
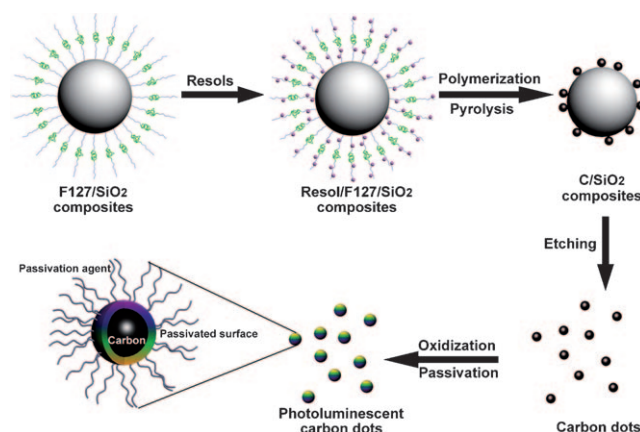


***Scheme 3.*** Synthesis of multicolor photoluminescent C-dots on silica sphere supports. Reprinted from Ref. [9] with permission.

Carbon precursor resols (phenol/formaldedyde resins, $M_w <$ 500) were introduced to these $F127/SiO_2$ composites and subsequently polymerized. The F127 surfactant phase was key in that it served as an anchor for the adsorption of resols through hydrogen bonding, so that polymerization took place on the shell of the $SiO_2$ sphere rather than in solution. Further heating of the composite to 900 °C in argon for 2 h led to C-dot/$SiO_2$ composites. The silica spheres were then removed by etching with 2 M NaOH solution, which released the C-dots. This route resulted in amorphous (possessing both $sp^2$ and $sp^3$ hybrids) C-dots 1.5–2.5 nm in size composed of 90.3 % C, 1.4 % H, and 8.3 % O (wt %). Carboxy groups were introduced on the C-dot surface by refluxing in 3 M $HNO_3$ for 24 h followed by neutralization and dialysis. FTIR confirmed the presence of carbonyl groups. The C-dots were then surface-passivated by ultrasonication with $PEG_{1500N}$ to form a homogeneous solution, followed by heating at 120 °C for 72 h. After surface passivation, the C-

dots produced $\lambda_{ex}$-dependent broadband PL emission with $\lambda_{em}$ maxima ranging from 400 to 580 nm.

Following a different approach, Giannelis and co-workers produced C-dots using NaY zeolites as supports.[2] The NaY zeolite was first ion-exchanged with 2,4-diaminophenol dihydrochloride followed by thermal oxidation at 300 °C in air for 2 h. It was found that ion exchange took place mostly at the surface of the zeolite as opposed to the interior, thereby resulting in C-dots decorating the surface of the zeolite after oxidation. The zeolitic material was then etched away by hydrofluoric acid to leave behind 4–6 nm sized C-dots that exhibited PL properties similar to those reported by using a nonsupported formation route.[3]

### 2.2.3. Synthesis with Microwaves and in Aqueous Solution

A facile microwave pyrolysis approach to synthesize C-dots was carried out by combining $PEG_{200}$ and a saccharide (for example, glucose, fructose) in water to form a transparent solution, followed by heating in a 500 W microwave oven for 2–10 min (Scheme 4).[20] The solution changed from colorless
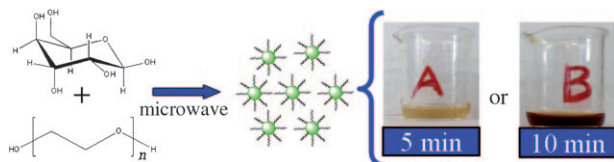


**Scheme 4.** Microwave approach to C-dot synthesis. Reproduced from Ref. [20] with permission.

to tan to dark brown over the time course of the reaction. The recovered C-dots exhibited sizes and PL properties related to the duration of the microwave heating. Longer heating times result in the C-dots enlarging slightly and emitting at longer wavelengths. For example, the average C-dot diameters were $(2.75 \pm 0.45)$ nm and $(3.65 \pm 0.6)$ nm for heating times of 5 and 10 minutes, respectively. When PEG was omitted, a similar color change was observed during microwave heating, but it is noteworthy that the nonpassivated particles expressed weak and irregular PL.

Most recently, Peng and Travas-Sejdic described a simple route to C-dots by using carbohydrates in aqueous solution.[23] The carbohydrates were first dehydrated using concentrated sulfuric acid to produce large carbonaceous materials. These materials were then ruptured into C-dots by refluxing in 2 M $HNO_3$. After cooling, the solution was neutralized by $Na_2CO_3$ solution and most of the water removed under vacuum. The C-dots were then dialyzed extensively to remove excess salts. The nonpassivated C-dots were 5 nm in size and exhibited a weak PL. The FTIR spectra revealed bands at 1572 cm$^{-1}$ and 1375 cm$^{-1}$, which were ascribed to C=C bond stretching and C−H vibrations, respectively. The C-dots were surface-passivated by treatment with 4,7,10-trioxa-1,13-tridecanediamine (TTDDA), ethylenediamine, oleylamine, or $PEG_{1500N}$ at 120 °C for 72 h under $N_2$. TEM analysis revealed a crystalline structure consisting of a lattice spacing close to that of turbostratic carbons. Concurrent XRD experiments

showed a diffraction peak corresponding to 3.4 Å ($d_{002}$). Elemental analysis showed O-rich C-dots comprised of 57.0 % C, 7.5 % H, 8.5 % N, and 27.0 % O (wt %).

### 2.3. C-Dot Nanocomposites

In the study by Sun et al., hybrid C-dots made by laser ablation of graphite were subsequently doped or coated with ZnO or ZnS.[11] The C-dots were first refluxed in 2.6 M $HNO_3$ for 12 h followed by extensive dialysis against large volumes of water and centrifugation (1000 g for 5 min) to remove any large particles. The supernatant was retained and the water evaporated to leave behind the oxidized C-dots. The 4–5 nm particles were then dispersed in DMF. To make ZnO/C-dots, zinc acetate was added to the C-dot dispersion under vigorous stirring followed by the dropwise addition of NaOH. The ZnO/C-dots were then recovered through centrifugation, repeatedly washed with water, and dried at 60 °C in a vacuum oven before final annealing at 200 °C for 2 h. ZnS/C-dots were similarly obtained by adding zinc acetate to a DMF dispersion of the C-dots followed by the slow addition of $Na_2S$ solution, centrifugation, and extensive washing of the ZnS/C-dot precipitate with water. Thermogravimetric analysis revealed the C/ZnO and C/ZnS molar ratios to be 20:1 and 13:1, respectively. ZnO and ZnS were found to incompletely coat the C-dot surface, thus leaving intact patches rich in carboxylic acid moieties which could then be functionalized by reaction with $PEG_{1500N}$. Interestingly, the Zn-based coatings afforded higher emission quantum yields than the uncoated C-dots, however, in both cases $PEG_{1500N}$ passivation was requisite for PL to occur.

Metal/C-dot nanocomposites were made by Tian et al. by reducing metal salts in the presence of C-dots generated from the oxidative etching of natural gas soot.[13] The metal ions, most likely bound to the peripheral carboxylic moieties by an ion-exchange process, were reduced to zero-valent metal upon addition of ascorbic acid and evolved into metal nanostructures. The resulting nanostructures were water soluble and, unlike the case of ZnO and ZnS[11] mentioned above, were far larger than the original C-dot: growing from 5 nm to 16–20 nm in size (Figure 6). Instead of the metal coating the C-dot, here the C-dots decorated the outside of the metal nanostructure. The metal particles appear to form chainlike structures embedded in a carbon matrix, thus supporting the hypothesis that the deposition of the metal nanoparticles was initiated from the C-dot surface.

### 2.4. Surface Functionalization

C-dots separated from SWCNTs produced by arc-discharge methods showed carbonyl functionalities at their surface, as evidenced by FTIR.[1] Other studies, including those of C-dots produced electrochemically from graphite[18] or by the chemical oxidation of candle soot,[10] showed similar results, with C-dots sporting COOH groups at their surface, as strongly evidenced by characteristic IR absorptions for $\tilde{\nu}$(C= O) around 1580 cm$^{-1}$ and 1630 cm$^{-1}$. Indeed, acid oxidative
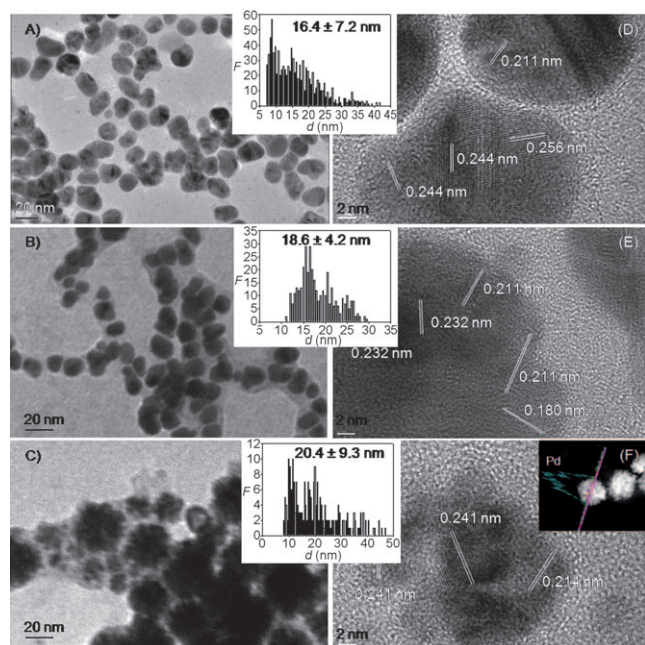
**Figure 6.** TEM micrographs of C-dots functionalized with A) Au, B) Cu, and C) Pd metal structures. Reprinted Ref. [10] with permission.

treatment, typically using $HNO_3$, readily introduces carbonyl functionalities at various carbon surfaces. The presence of these groups renders the C-dots water soluble, which is essential for biologically motivated work, and simultaneously furnishes a convenient handle for subsequent surface functionalization, which can be realized easily using well-established conjugation protocols.

By using different surface passivation agents, one can also impart solubility in non-aqueous solvents and significantly modify the PL properties of the C-dots. Typically, the attachment of amino-terminated reagents (for example, ethanolamine, $PEG_{1500N}$), which leads to the formation of amide linkages, is used for the surface passivation of C-dots. As noted earlier, some one-step methods for the formation of C-dots allow for the direct incorporation of the surface functionality of choice by their introduction during C-dot generation, without the need for later modification steps.[2,3,6,8]

## 3. Physical and Chemical Properties

### 3.1. Crystalline Nature and Hybridization

Selected-area electron-diffraction (SAED) experiments on C-dots with a size of about 3 nm prepared by a one-step laser ablation/passivation method[6] revealed a ring pattern, with the ratio of the squares of the ring radii being 3:8:11:16:19. This implies a diamond-like structure, with the rings respectively corresponding to the (111), (220), (311), (400), and (331) planes of diamond. This apparent structure was observed whether or not the C-dot was synthesized in $PEG_{200N}$ as the passivating ligand or in water (where methyl groups are found at the surface of the final particles). The

lattice spacings observed varied from 0.2–0.23 nm and are, in fact, quite close to the (100) facet of graphite. We note that the lattice fringes of the diffraction planes of diamond-like and graphitic carbon lie very close to one other, thus rendering unambiguous assignment difficult without other corroborating evidence. Unfortunately, no further studies were done to study the hybridization of the carbon or the elemental composition in these C-dots, aside from surface measurements.

Similarly, Ray et al. reported lattice spacings of 0.208 nm for C-dots made from oxidizing candle soot, thus also suggesting $sp^3$ diamond-like carbon or $sp^2$ graphitic carbon.[10] By using $^{13}C$ NMR studies, they were able to confirm the presence of $sp^2$ carbon with signals in the $\delta = 90$–180 ppm range, while the absence of signals in the $\delta = 8$–80 ppm range led to the assertion of a lack of detectable $sp^3$ carbon (Figure 7). Furthermore, FTIR measurements also confirmed the presence of C=C aromatic ring stretches. Therefore, they concluded that their C-dots consisted of a nanocrystalline core of graphitic $sp^2$ carbon atoms functionalized with peripheral carboxylic/carbonyl moieties.
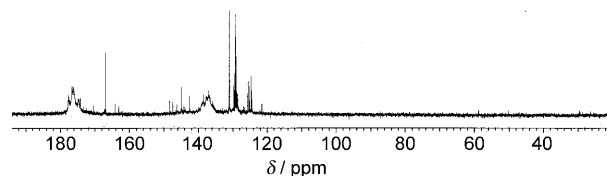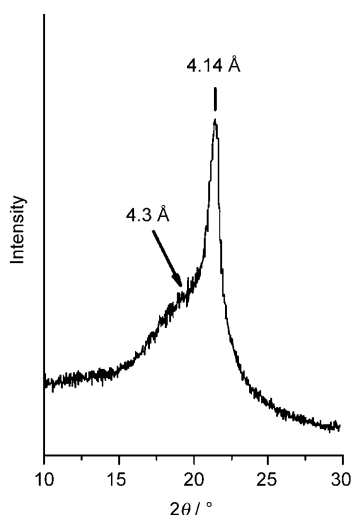


**Figure 7.** $^{13}C$ NMR spectrum of C-dots in $D_2O$ showing the presence of $sp^2$ carbon atoms. Reprinted from Ref. [13] with permission.

C-dots ($2.8 \pm 0.5$ nm) produced by electrochemical oxidation of MWCNTs were graphitic in nature with lattice spacings of 3.3 Å (HRTEM determined), which is close to the (002) facet of graphite.[19] Raman spectra showed characteristics of both $sp^2$ and disordered carbon. Similarly, C-dots produced from the electrochemical oxidation of graphite, when examined by HRTEM, showed lattice spacings of 3.28 Å.[17] When produced electrooxidatively from graphite in the water-miscible IL [bmim][BF4], 8–10 nm C-dots also showed lattice spacings of 0.21–0.25 nm indicating the (100) facet of graphite at high water contents, and 0.33 nm when the water content was below 10%.[8]

One-step thermal decomposition reactions of citrate salts produced C-dots with a size of 7 nm, whose XRD patterns were indicative of disordered carbon alongside the respective passivation agent.[3] As shown in Figure 8, the XRD pattern of C-dots made from octadecylammonium citrate, for example, gives two superimposed broad reflections: a broad one centered at 4.3 Å and a sharper peak at 4.14 Å which is indicative of disordered carbon and densely packed alkyl groups arising from the octadecyl chains, respectively.

Raman studies of 5 nm C-dots produced by laser ablation show contributions from both the G band at 1590 cm$^{-1}$, related to in-plane vibration of $sp^2$ carbon, and the D band at

**6734** www.angewandte.org

© 2010 Wiley-VCH Verlag GmbH & Co. KGaA, Weinheim

*Angew. Chem. Int. Ed.* **2010**, *49*, 6726–6744

**Figure 8.** XRD pattern of octadecyl-functionalized C-dots. Reprinted from Ref. [3] with permission.

1320 cm$^{-1}$, related to the presence of sp$^3$ defects. However, HRTEM images generally suggested amorphous carbon unless C-dots were coated with ZnS.[11] Raman studies of C-dots produced by the oxidation of candle soot[10] and by electrochemical means[8,19] also showed both the D and G bands (Figure 9). The ratio of the intensities ($I_D/I_G$) of these characteristic bands can be used to correlate the structural properties of the carbon. In the case of C-dots produced electrochemically from MWCNTs,[19] the resulting ratio of 2 indicates nanocrystalline graphite.

Taken together, it can generally be concluded that C-dots consist of an amorphous to nanocrystalline core with predominantly sp$^2$ carbon; the lattice spacings are consistent with graphitic or turbostratic carbon. Unless otherwise modified,
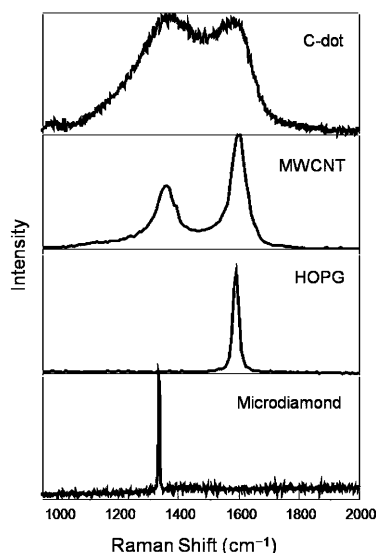


**Figure 9.** Raman spectra of C-dots, MWCNTs, highly ordered pyrolytic graphite (HOPG), and microdiamond powder. Reprinted from Ref. [19] with permission.

oxidized C-dots generally feature carboxylic moieties at their surface, with overall oxygen contents ranging anywhere from 5–50 wt%, depending upon the exact experimental conditions used.

### 3.2. Optical Properties
#### 3.2.1. Absorbance and Photoluminescence

C-dots typically show strong optical absorption in the UV region, with a tail extending out into the visible range (see Figures 10 and 12–14 for representative spectra). C-dots produced from a one-step laser-passivation method have an excitation edge at 280 nm (4.4 eV).[6] C-dots (2.8 ± 0.5 nm) produced from electrochemical oxidation of MWCNTs show an absorption band at 270 nm, with a narrow full width at half maximum (FWHM) of 50 nm.[19] This is similar to microwave-produced C-dots (3 nm) which had an absorption band at 280 nm, also with a FWHM of 50 nm.[20] After surface passivation with TTDDA, C-dot absorbance was found to increase in the 350 to 550 nm range.[23]

One of the most fascinating features of C-dots, both from fundamental and application-oriented stances, is their PL. Since C-dots have only recently emerged in the literature, knowledge into the origins of their PL is a matter of current debate and requires greater clarification. In any case, one unifying feature of the PL of C-dots is the clear $\lambda_{ex}$ dependence of the emission wavelength and intensity. Whether this occurs because of optical selection of differently sized nanoparticles (quantum effect) and/or different emissive traps on the C-dot surface or another mechanism altogether is currently unresolved. Similarly, the requirement for surface passivation is poorly understood, but appears to be linked to the fabrication method employed. For example, C-dots produced by laser ablation showed PL emission only after surface passivation by certain organic moieties, whether suspended in solution or in the solid state. The resulting PL emission spectra ranged from the visible into the near-infrared (NIR), were generally spectrally broad, and depended upon $\lambda_{ex}$ (Figures 10 and 11).[12]

This behavior is similar to their Si nanocrystal counterparts[29] and may reflect not only effects from particles of different sizes in the sample but also a distribution of different emissive sites on each C-dot. Mechanistically, Sun et al. attribute the PL to the presence of surface energy traps that become emissive upon surface passivation.[12] They concluded that there must be a quantum confinement of emissive energy traps to the particle surface for the particle to exhibit strong PL upon surface passivation. A similar effect is seen for Si nanocrystals, for which a widely accepted mechanism for luminescence emission is the radiative recombination of excitons.[29] When coated with ZnO or ZnS, the C-dots produced by Sun et al. still required further passivation by PEG$_{1500N}$ for PL to occur (Figure 12).[11] However, Ag, Cu, or Pd metal nanocomposites of C-dots, made from oxidized natural gas soot, required no further passivation for observation of PL: PL excitation and emission spectrum were observed that were red-shifted about 30 nm from the purely oxidized C-dots.[13]
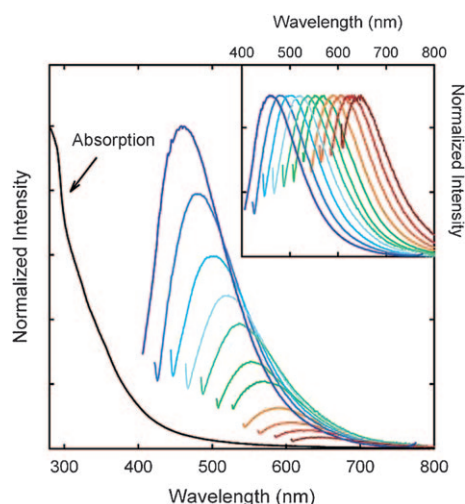
**Figure 10.** Absorbance and luminescence spectra with increasingly longer excitation wavelengths (in 20 nm increments starting from 400) of 5 nm PPEI-EI C-dots in aqueous solution formed from laser ablation methods. Reprinted from Ref. [12] with permission.
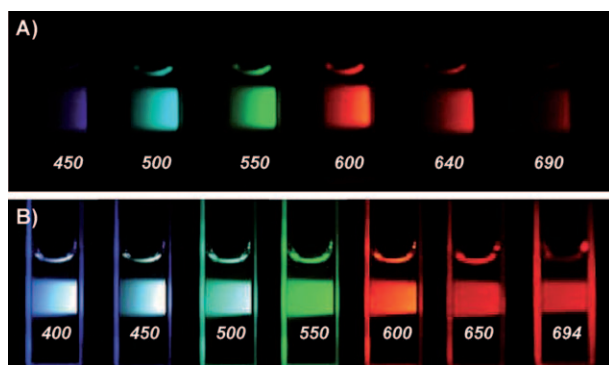


**Figure 11.** Aqueous solution of C-dots passivated with PEG$_{1500N}$ A) excited at 400 nm and photographed through band-pass filters of different wavelengths as indicated, and B) excited at the indicated wavelengths and photographed directly. Reprinted from Ref. [12] with permission.

Another laser ablation method produced similar results in terms of surface passivation being required for PL to occur.[6] In this study, PL occurred when C-dots formed directly in the presence of PEG$_{200N}$ were excited at 420 nm. However, no PL occurred when C-dots were formed in water and only methyl and few carboxylic moieties were present on the surface. Only minimal PL resulted even after oxidation in perchloric acid to produce many more carboxylic moieties at the surface. Only by subsequent passivation by incubation in PEG$_{200N}$ were these C-dots capable of producing strong PL emission. The $\lambda_{ex}$ and $\lambda_{em}$ maxima were red-shifted upon increasing the MW of the PEG used. The use of two different C-dot starting materials, graphite and carbon black, produced no notable changes in the final C-dot properties. However, for this fabrication method, no studies were done to determine if the C-dot emission was dependent upon $\lambda_{ex}$.

C-dots ($2.8 \pm 0.5$ nm) prepared by electrochemical oxidation of MWCNTs, exhibit blue PL centered at 410 nm when
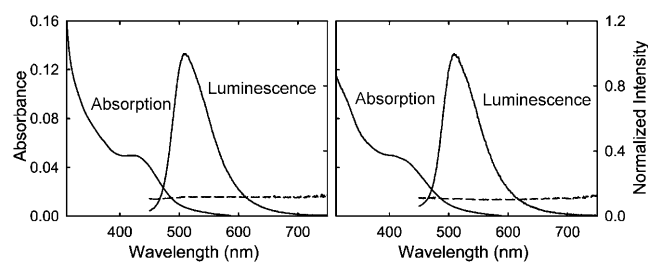


**Figure 12.** Absorption and luminescence emission spectra (440 nm excitation) of PEG-passivated ZnS/C-dots (left) and ZnO/C-dots (right) in aqueous solutions (solid lines). As also shown for comparison, the carbon nanoparticles doped with ZnS or ZnO but without PEGs were not emissive (dashed lines, magnified ×10 and offset by 0.1 for easier viewing). Reprinted from Ref. [11] with permission.

excited at 365 nm.[19] These C-dots also showed $\lambda_{ex}$-dependent emission but, interestingly, no additional passivation step was required here for PL to occur. At this time, it is unclear why this would be the case or whether TBA$^+$ ions might serve as passivating agents. Yet another report on electrochemical C-dot synthesis did not comment on whether the PL showed $\lambda_{ex}$ dependence, but further surface passivation was not required for PL to occur in this case either.[18]

Similarly, C-dots produced from the oxidation of candle soot contained an abundance of carbonyl groups at their surface and required no further functionalization for PL to occur.[7,10] Although their excitation spectra differed little, their PL emission spectra were strongly linked to their electrophoretic mobilities (Figure 4). At this time, it is not entirely clear whether size or surface charge effects were most responsible for the observed C-dot mobilities. The PL spectra have a broad color range, with peak intensity wavelengths ranging from 415–615 nm. The FWHM broadens as the emission red-shifts, perhaps because of incomplete size separation.

An SiO$_2$-supported route to 1.5–2 nm C-dots required surface passivation for PL to occur, with the PL showing marked $\lambda_{ex}$ dependence.[9] When produced by microwave synthesis of saccharides in PEG$_{200}$, the resulting 3 nm C-dots also exhibited $\lambda_{ex}$ dependence.[20] These C-dots gave broad emission, with an emission maximum at 425 nm when excited at 330 nm. The PEG$_{200}$ was essential for PL to occur here as well, but some COOH functionality was still retained at the C-dot surface, as evident by FTIR analysis.

C-dots (7 nm) made from the one-step thermal decomposition of ammonium salts or 4-aminoantipyrine compounds showed emission that depended very strongly on the $\lambda_{ex}$.[2,3] In fact, those C-dots made from the carbonization of 2-(2-aminoethoxy)ethanol citrate salt[3] or 11-aminoundecanoate citrate salt[2] are among those emitting the most red-shifted PL of any covered in this Review (Figure 13, for example).

For C-dots produced electrochemically in water-rich ILs, the resulting 8–10 nm particles were oxidized at the surface and had a $\lambda_{em}$ maximum at 364 nm when excited at 260 nm. However, when the water content was very low ($< 10\%$), the 2–4 nm C-dots produced were found to be functionalized by the IL and had higher quantum yields (2.8–5.2%) than the
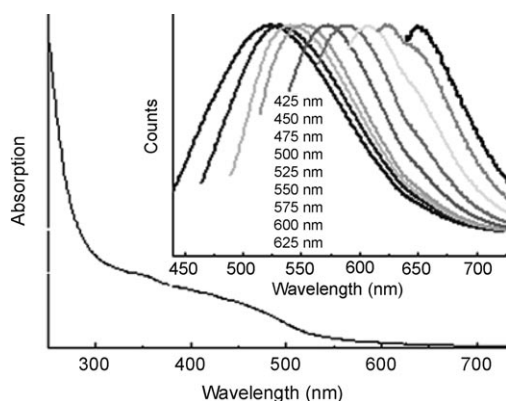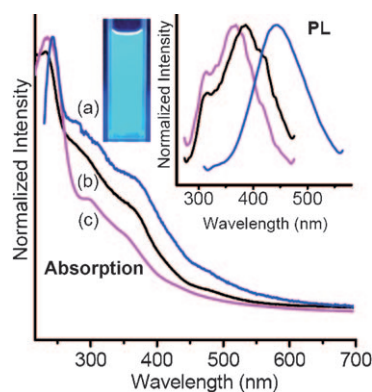
**Figure 13.** Absorption and normalized PL spectra at different excitation wavelengths of hydrophilic C-dots made from thermal decomposition of 2-(2-aminoethoxy)ethanol citrate salt. Reproduced from Ref. [3] with permission.



**Figure 14.** UV absorption and PL of C-dots electrochemically exfoliated using IL electrolytes containing different water contents. The emission spectra were excited using 260 nm light: a) 10 wt% water(blue curve); b) 60 wt% water(black curve); c) 90 wt% water (pink curve). A blue shift of the emission is apparent with higher wt% of water in the electrolyte. Reproduced from Ref. [8] with permission.

larger particles. Interestingly, the PL of the larger C-dots was centered at 364 nm while that of the smaller ones was at 440 nm, which is contrary to what would be expected based solely on quantum confinement effects. Additionally, the IL-functionalized C-dots gave broad, structureless PL between 400 and 600 nm, whereas the larger nonfunctionalized C-dots had notable features in their emission profiles (Figure 14). These results highlight how the surface chemistry can significantly affect the PL properties of C-dots. This is also true for the quantum yield, as is discussed below.
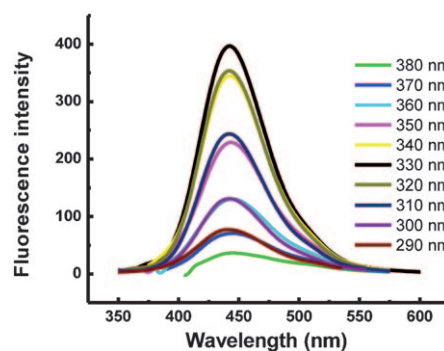
Notably, when produced by electrochemical oxidation of graphite and further size selected into $(1.9 \pm 0.3)$ and $(3.2 \pm 0.5)$ nm fractions by MW cut-off membranes, C-dots were claimed to show size-dependent but $\lambda_{ex}$-independent emissions (Figure 15).[17] Zhao et al. argue that the dependency of the C-dot PL on the excitation wavelength is due solely to size differences rather than different emissive trap sites on similarly sized particles. However, this is the only such claim on this topic, with the lion's share of the evidence pointing toward quantum effects and/or different surface trap sites causing a $\lambda_{ex}$ dependency.

The quantum yield of C-dots varies with the fabrication method and the surface chemistry involved. C-dots of about 5 nm in size, produced by laser ablation had quantum yields between 4 and 10%, depending on the excitation wavelength.[12] These are in the same range as similarly sized Si nanocrystals.[29] In contrast, 7 nm C-dots produced using one-step thermal decomposition methods gave a quantum yield of only 3%, but were essentially independent of $\lambda_{ex}$; interestingly, electron paramagnetic resonance spectra showed the presence of radicals as defect sites.[3] Smaller 4–6 nm C-dots made by thermal decomposition on NaY supports resulted in a more blue-shifted emission (as expected based on quantum confinement effects) and even lower quantum yield.[2]

The quantum yield of C-dots was found to be dependent on surface passivation in many studies.[6,11,12,23] C-dots from laser ablation methods passivated with PPEI-EI had lower quantum yields than those passivated with PEG$_{1500N}$.[12] However, when the PPEI-EI was removed and replaced with PEG$_{1500N}$, the quantum yield recovered. When coated



**Figure 15.** PL of 1.9 nm C-dots at different excitation wavelengths of 290–380 nm. Reprinted from Ref. [17] with permission.

with ZnO or ZnS and PEG$_{1500N}$, the quantum yield (440 nm excitation) increases substantially to 45 and 50%, respectively.[11] Yet these values differed as much as 15% from batch to batch. While the role the Zn-based coating plays in enhancing the quantum yield is still unclear, one proposal is that it may provide a secondary, more effective surface passivation in combination with the PEG passivation agent. C-dot/metal nanocomposites made using 4.8 nm C-dots produced by the oxidation of natural gas soot also resulted in a substantial increase in the quantum yield from 0.43% for C-dots covered with COOH functionalities to 60.1%, 33.4%, and 36.7% for C-dot nanocomposites made with Cu, Pd, and Ag, respectively.[13]

Effects of passivation on quantum yield were also seen for C-dots produced in a one-step laser ablation/passivation protocol where the quantum yield ranged from 3 to 8%, depending on the passivation agent used (diamine hydrate: 3.7%, PEG$_{200N}$: 5.0%, and diethanolamine: 7.8%).[6] Methods producing C-dots with only COOH groups at the surface resulted in quantum yields of 6.4%,[19] 1.2%,[17] 0.8%,[7] 1.9%,[7] and 0.43%,[13] which are typically lower than those passivated by organic ligands. C-dots made from dehydrated carbohydrates were found to be weakly emissive after

oxidation with nitric acid, with the PL becoming more intense once the surface was passivated with an organic molecule or polymer.[23] Again, the quantum yield was found to be dependent on the passivation agent used and was the highest (13%) when TTDDA was used. In general, while some C-dots exhibit PL with only carboxylic moieties at their surface, their quantum yields can typically be increased by further surface passivation and is particularly high when the C-dot has a metal-containing shell or is associated with a metal-based nanostructure.

C-dots have shown high photostability in studies to date.[12,17,23] A recent laser scanning confocal microscopy study showed that neither blinking nor meaningful reduction in the PL intensity were observed during several hours of continuous exposure to excitation.[12] Accordingly, C-dots produced by electrooxidation of graphite showed no appreciable changes in the PL intensity even after continuous exposure to a Xe lamp (8.3 W) for 6 h (Figure 16).[17] Only a 17% decrease in the PL intensity for C-dots made from carbohydrates was seen after 19 h of continuous excitation at 360 nm.[23]
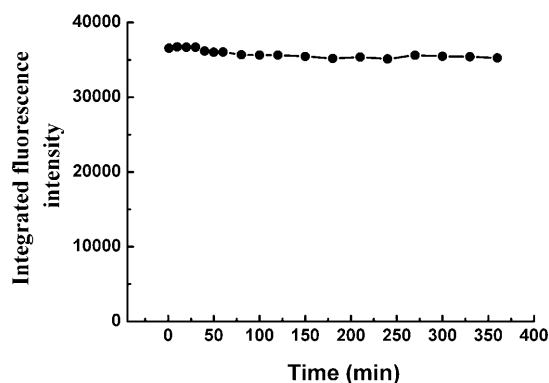


***Figure 16.*** Dependence of fluorescence intensity on the excitation time for 1.9 nm C-dots in ultrapure water. Reproduced from Ref. [17] with permission.

Luminescence decays from laser ablation-produced C-dots, excited at 407 nm, have multiexpotential PL decays with average excited-state lifetimes of 5 ns for emission at 450 nm and 4.4 ns for emission at 640 nm.[12] The multiexponential nature of the lifetime suggests that different emissive sites are present. Microwave-synthesized C-dots about 3 nm in size were found to have a mean PL lifetime of $(8.7 \pm 0.05)$ ns.[20]

Ionic strength and pH values are known to affect the fluorescence properties of different molecules and nanoparticles.[35] A dependence of the C-dot PL intensity on the pH value was seen in a few studies.[7,9,17] For example, Zhao et al. found the intensity decreased when the pH value of the solution was higher or lower than 4.5, yet totally recovered when the pH value was adjusted back to this optimal value (Figure 17). At the same time, a slight shift in the emission peak was found with variation in the pH value. Liu et al. observed the greatest PL intensity of C-dots derived from candle soot to occur at pH 7, with the intensity decreasing significantly by 40–89% and with a slight blue shift upon
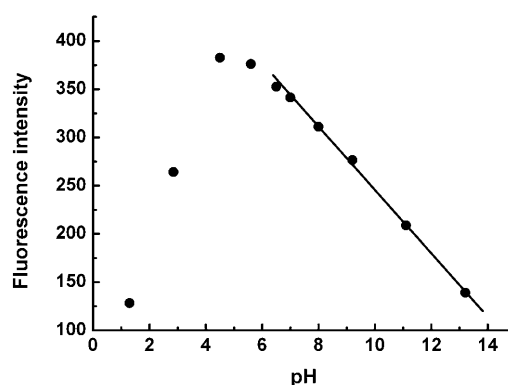


***Figure 17.*** Effect of solution pH value on C-dot fluorescence intensity. Reproduced from Ref. [17] with permission.

changing to either an acidic or basic solution.[7] Others found only a decrease of about 3% in the quantum yield on going from a neutral pH value to pH 5 or 9.[9]

C-dots, ZnO/C-dots, and ZnS/C-dots exhibit strong PL upon two-photon excitation in the NIR region, with an estimated two-photon absorption cross-sections comparable to those of available high-performance semiconductor QDs.[4,11] The two-photon experiments were conducted on C-dots deposited on glass substrates. A quadratic relationship between the excitation laser power and the C-dot PL intensity was found by using a femtosecond pulsed Ti:sapphire laser at 800 nm at different powers, thus confirming the two-photon excitation of the C-dots. The two-photon absorption cross-section was determined to be $(39000 \pm 5000)$ GM (Goeppert-Mayer unit; $1 \text{ GM} = 10^{-50} \text{ cm}^4 \text{ s photon}^{-1}$) at 800 nm excitation. This value falls between that reported for CdSe quantum dots (780–10300 GM)[36] and CdSe/ZnS core-shell quantum dots ($\approx 50000$ GM)[37] for the same excitation wavelength. The two-photon excited C-dot emission profile has a bandwidth comparable to the one-photon spectrum of C-dots on glass substrates, but is considerably narrower than the one-photon emission spectra of C-dots in aqueous solution. This observation indicates that immobilization may influence the emission properties of the C-dots. The C-dots, ZnO/C-dots, and ZnS/C-dots have also proven useful for cellular imaging using two-photon luminescence microscopy (See Section 4.1).

### 3.2.3. Photoinduced Electron Transfer and Redox Properties

C-dots (ca. 4.2 nm) produced by laser ablation methods were shown to be both excellent electron donors and acceptors.[14] Their PL emission ($\lambda_{ex} = 425$ nm) in toluene was quenched by the electron acceptors 4-nitrotoluene ($-1.19$ V versus NHE) and 2,4-dinitrotoluene ($-0.9$ V versus NHE). The obtained Stern–Volmer quenching constants ($K_{SV} = \tau_0 k_q$) of $38 \text{ M}^{-1}$ and $83 \text{ M}^{-1}$ for 4-nitrotoluene and 2,4-dinitrotoluene, respectively, indicate the latter to be the more effective quencher as expected because of its stronger electron-acceptor capability. On average (because of the multiexponential C-dot luminescence decay), the biomolecular rate constants $k_q$ from 4-nitrotoluene and 2,4-dinitrotoluene quenching were $9.5 \times 10^9 \text{ M}^{-1} \text{ s}^{-1}$ and $2.1 \times 10^{10} \text{ M}^{-1} \text{ s}^{-1}$, respec-

tively. These values are beyond the upper limit for such quenching processes in solution, thus suggesting the high efficiency of the underlying electron-transfer process as well as static quenching effects. Once static quenching effects are taken into account, these quenching rate constants are still at the diffusion-controlled limit for dynamical quenching, thus proving that C-dots can act as very efficient electron donors.

Additionally, C-dots can serve as strong electron acceptors, and can quench the luminescence of known electron donors such as *N,N*-diethylaniline (0.88 V versus NHE) highly efficiently. This behavior is solvent-dependent and is more efficient in polar solvents, which is indicative of an electron transfer quenching mechanism.

### 3.2.4. Electrochemical Luminescence

Since semiconductor nanocrystals are well known to exhibit electrochemiluminescence (ECL),[38,39] it comes as no surprise that C-dots have aroused interest for ECL studies.[18,20] The ECL emission of C-dots (ca. 2.0 nm) produced from the electrochemical oxidation of graphite was observed as the potential was cycled between $+1.8$ and $-1.5$ V (Figure 18).[18]
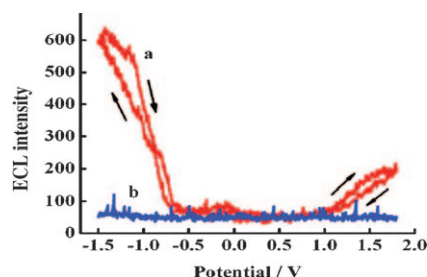


*Figure 18.* ECL responses a) with and b) without C-dots at a Pt electrode in 0.1 M phosphate buffer solution (pH 7.0) with a scan rate of 0.1 V s$^{-1}$. Reproduced from Ref. [18] with permission.

The suggested ECL mechanism involves the formation of excited-state C-dots (R*) by electron-transfer annihilation of negatively charged (R$^{\bullet-}$) and positively charged (R$^{\bullet+}$) species (ET1 route in Figure 19). R$^{\bullet+}$ is the more stable of the two species, as indicated by the greater intensity of the cathodic ECL (Figure 18). Interestingly, when produced by microwave synthesis, 3 nm PEG$_{200}$-functionalized C-dots also exhibited ECL behavior, but the R$^{\bullet-}$ species was found to be more stable in this case.[20] The presence of peroxydisulfate (S$_2$O$_8^{2-}$)
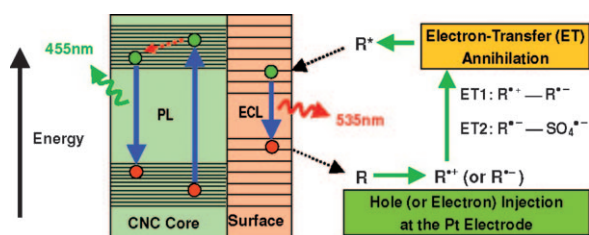


*Figure 19.* The ECL and PL mechanisms in C-dots. Reproduced from Ref. [18] with permission.

enhanced the ECL (ET2 route in Figure 19) in the cathodic potential range and produced a stable and sensitive (as no other co-reactants tested elicited an ECL enhancement) ECL response, thus suggesting the application of C-dots for ECL sensing.[18]

As ECL is mainly characterized by surface-state transitions in nanoparticles (whereas in nanoparticles, PL is more reminiscent of the core state), comparison between the ECL and the PL of nanoparticles is an excellent way to investigate the presence of surface traps.[40–42] When excited at 330 nm, the PL emission of the C-dot was centered at 455 nm, while the ECL emission was centered at 535 nm.[18] This substantial red-shift indicates that the emitting states are different, thereby signifying the presence of surface traps with incomplete passivation. If the particle were more completely passivated, the ECL profile would resemble the PL spectrum, as seen in the case of CdSe/ZnSe core/shell nanoparticles.[41] Further support for this notion is provided by the persistence of the red-edge tail in the PL emission spectrum for many C-dots, which indicates emission from incompletely-passivated surface traps (see Figures 10 and 12–14).[40–42] The C-dot particles in these ECL studies contain COOH groups at their surfaces, as shown by FTIR results.[18]

On the basis of ECL evidence implying the presence of surface trap states, coupled with the pervasive size and $\lambda_{ex}$ dependency of C-dot PL, we postulate that C-dots feature core band gaps that are dependent on the size, with the most intense PL attributable to the direct recombination of electron-holes whereas the less intense bands (those further red-shifted) may be assigned to surface-state traps and phonon-assisted recombination similar to observations in Si nanocrystals.[42] Experiments aimed at investigating the effects of different surface capping agents on the ECL of C-dots would prove invaluable for elucidating the effects of surface passivation on surface traps. It would also be interesting to determine whether the ECL of C-dots is size-independent, as is the case for Si nanocrystals.[42]

### 3.3. Cytotoxicity

The toxicity of C-dots is a natural concern because of their potential for bioimaging and nanoscale dimensions. Toxicity studies have been conducted by various research groups, and while the reports are few at the moment, C-dots appear to have low toxicity.[10,15,16] Ray et al. performed cell viability tests on HepG2 cells, a human hepatocellular liver carcinoma line, using MTT and Trypan blue assays. The cells were exposed to 0.1–1 mg mL$^{-1}$ of C-dots, 2–6 nm in size extracted from candle soot, for 24 h. The cell survival rate was then determined by absorbance at 550 nm by using the MTT assay or cell staining/counting methods for the Trypan Blue assay. The cell survival rate for a C-dot exposure of less than 0.5 mg mL$^{-1}$ ranged between 90 and 100% (Figure 20). At C-dot concentrations above 0.5 mg mL$^{-1}$, the survival rate drops to about 75%; however, the highest levels investigated were $10^2$ to $10^3$ times higher than necessary for bioimaging studies, thus suggesting that C-dots pose minimal toxicity effects at useful concentrations for bioimaging.
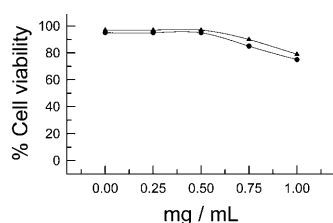
**Figure 20.** Cell viability study of HepG2 cells exposed to 0.1–1 mg mL$^{-1}$ C-dots. ▲ MTT, ● Tryptan Blue. Reproduced from Ref. [10] with permission.

Sun and co-workers have also studied the in vitro cytotoxicity of C-dots as well as their in vivo effects.[15,16] Trypan Blue and MTT assays of human breast cancer MCF-7 and human colorectal adenocarcinoma HT-29 cells after exposure to C-dots (ca. 5 nm, produced from laser ablation and surface passivation with PEG$_{1500N}$) were conducted to determine cell mortality, proliferation, and viability. Their results for both cell lines were similar to those reported by Ray et al.,[10] but found, in general, greater than 80% cell viability rate for C-dot concentrations up to 0.1 mg mL$^{-1}$. Similarly, Zhao et al. showed cell viability of 293T human kidney cells to be above 80% for up to 400 ug mL$^{-1}$ of electrochemically oxidized C-dots (without PEG passivation).[17]

Additionally, Sun and co-workers performed in vivo studies using CD-1 mice.[16] The mice, divided into three groups, were exposed intravenously to either 8 or 40 mg of C-dots (ca. 5 nm, PEG$_{1500N}$ passivated) or 0.9% NaCl aqueous solution (nontoxic control). At 1, 7, and 28 days postexposure, mice were sacrificed and blood and organ samples taken for toxicological assays. During the 4 week period, no mice exposed to C-dots exhibited any adverse clinical signs or abnormal food intake. Hepatic indicators, kidney function, uric acid, blood urea nitrogen, and creatinine were all at similar levels for mice exposed to different dosages of C-dots and the NaCl control, thus suggesting the nontoxicity of C-dots at exposure levels and times beyond those typically used for optical in vivo imaging studies. Harvested organs also exhibited no abnormalities or necrosis. While the amount of C-dots found in the liver and spleen were higher than those found in other organs, the accumulations were relatively minor and no organ damage was present.

All the evidence points to the great potential of C-dots for in vitro and in vivo imaging studies. Although more toxicity studies need to be carried out, such as LD$_{50}$ (median lethal dose) measurements, some researchers predict that the biocompatibility of C-dots will be similar to that of current FDA-approved dyes used as optical imaging agents such as indocyanine green (LD$_{50}$ = 60 mg kg$^{-1}$ body weight).[16]

## 4. Applications

### 4.1. Bioimaging

Quantum dots such as CdSe and related core-shell nanoparticles have been used in various in vitro and in vivo

optical imaging experiments.[43–45] However, since heavy metals are the essential elements in such QDs dots, they have prompted serious health and environmental concerns.[44] As a consequence of their tunable PL properties and established low toxicity, C-dots form an attractive alternative for bioimaging applications.

Sun and co-workers reported the first study on C-dot bioimaging capabilities, which was followed by many other studies.[4,12,15,16] They demonstrated the potential of C-dots passivated with PPEI-EI for two-photon luminescence microscopy using human breast cancer MCF-7 cells.[4] After incubation of the cells with C-dots for 2 h at 37°C followed by washing to remove any extracellular C-dots, they exhibited bright luminescence in both the cell membrane and cytoplasm regions when imaged using a fluorescence microscope with excitation by 800 nm laser pulses (Figure 21). The ability of
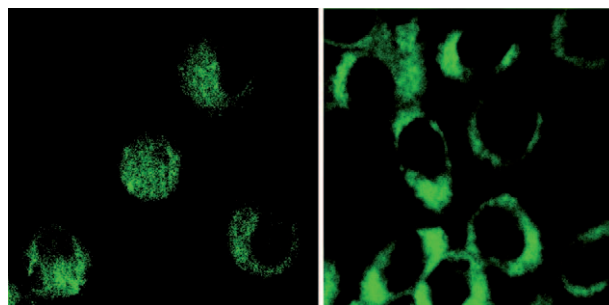


**Figure 21.** Two-photon luminescence image of human breast cancer MCF-7 cells with internalized C-dots passivated with PPEI-EI. Reprinted from Ref. [4] with permission.

the cells to uptake C-dots was found to be temperature-dependent, with no C-dots internalized at 4°C. Notably, although the C-dots were likely internalized into the cell through endocytosis, the cell nucleus was not infiltrated significantly.

Ray et al.[10] also used C-dots for conventional bioimaging by incubating a ≈107 cell mL$^{-1}$ solution of Ehrlich ascites carcinoma cells (EACs) with an aqueous solution of C-dots for 30 minutes. The C-dots were produced by burning a candle, chemically oxidizing the soot, and then separating out the 2–6 nm C-dots. The labeled cells were separated from any free C-dots still in solution through centrifugation and resuspended in phosphate buffer. A drop of this suspension was then imaged under an Olympus IX71 fluorescence microscope equipped with a digital camera. Figure 22 demonstrates the ability of C-dots to penetrate into the cells without any further surface passivation of the C-dots following acidic oxidation. Liu et al. also found 1.5–2 nm C-dots uptake into *E. coli* and murine P19 progenitor cells and could be further imaged using laser scanning confocal microscopy. The PL of the C-dot could be excited over a broad range of 458–514 nm, and showed high photostability, no blinking, and low photobleaching.[9]

Elucidating the exact mechanism of C-dot uptake by cells still requires more investigations, but evidence to date suggests an endocytosis mechanism. In the future, better
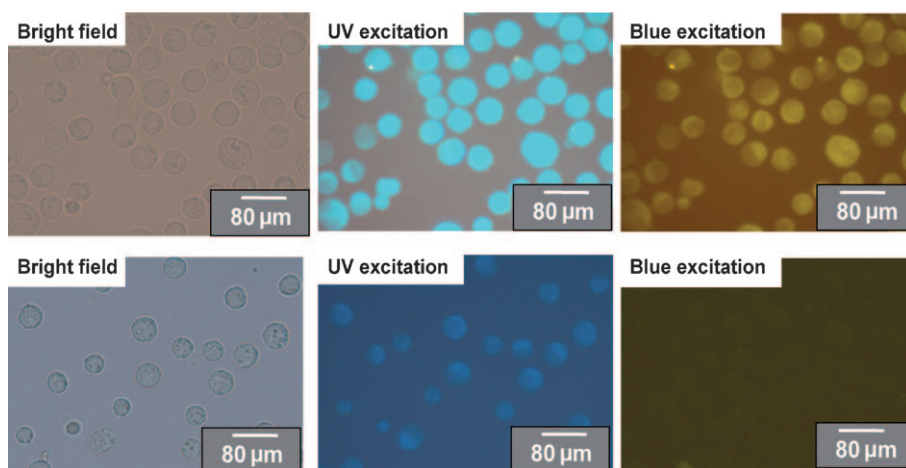
**Figure 22.** Fluorescent C-dot labeling of EAC cells. Washed cells were imaged under bright field, UV, and blue light excitations. The bottom row images correspond to the control experiment where no C-dots were used. Cells become bright blue-green under UV excitations and yellow under blue excitation but were colorless in the control sample. The light blue color of the control sample under UV excitation is due to the well-known autofluorescence of cells. Reprinted from Ref. [10] with permission.

Wang et al. demonstrated the photoreduction of $Ag^+$ to elemental Ag by photoirradiating an aqueous solution of C-dots (ca. 5 nm, fabricated by laser ablation methods) and $AgNO_3$ using a monochromator-filtered Xe arc lamp with excitation at 450 or 600 nm.[14] The formation of Ag was evidenced by the emergence and rapid growth of a surface plasmon band absorbance for nanoscale Ag. Unfortunately, no further characterization of the Ag nanostructures formed was undertaken. In a control experiment, no Ag formed when the experiment was repeated in the absence of the C-dots in solution.

accumulation of C-dots in the cell and perhaps even the nucleus may be achieved by attaching the C-dot to facilitator proteins or peptides which cross cell membrane barriers more readily.

In vivo studies of optical imaging using C-dots (ca. 5 nm) produced by laser ablation have also been demonstrated.[15] In vivo fluorescent contrast agents are ideally bright, non-toxic, biocompatible, and stable against photobleaching. Both C-dots and ZnS-doped C-dots functionalized with $PEG_{1500N}$ were injected by three different routes (subcutaneously, intradermally, and intravenously) into female DBA/1 mice. Both types of C-dots could be excited through 470 nm and 545 nm filters. The ZnS-doped C-dots emitted more strongly than nondoped C-dots, which is consistent with their PL behavior in solution. The PL from both types of injected dots faded 24 h after injection. After intradermal injection into the front extremity, the C-dots migrated to the axillary lymph nodes, similar to CdSe/ZnS semiconductor quantum dots, but at a slower rate, presumably because of PEG functionalization reducing their interaction with lymph cells. When injected intravenously for whole-body circulation studies (Figure 23), C-dot emission from the bladder area was observed, and 3 h after injection PL could be detected in the urine. At 4 h after injection, organs were harvested and the C-dots were found to have accumulated in the kidney (which is consistent with a urine excretion pathway) and scantly in the liver. Although significant hepatic uptake is known for nanoparticles and nanotubes,[46] the lower levels observed for C-dots was attributed to the surface PEG likely reducing their protein affinity.

### 4.2. Photoreduction of Metals

The electron-donor capabilities of photoexcited C-dots have clear potential in reduction reactions. For example,
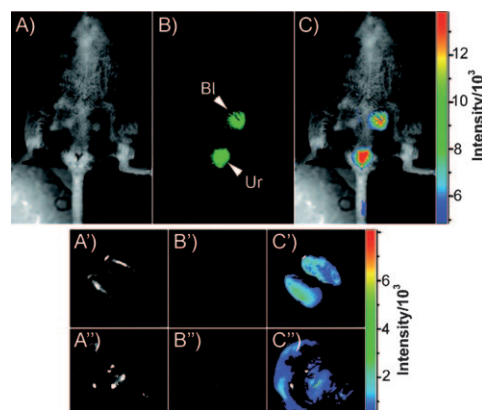


**Figure 23.** Intravenous injection of C-dots: A) bright field, B) as-detected fluorescence (Bl, bladder; Ur, urine), and C) color-coded images. The same order is used for the images of the dissected kidneys (A'–C') and liver (A''–C''). Reproduced from Ref. [15] with permission.

### 5. Graphene-Derived Luminescent Carbons

Although less explored, the graphenes and their chemical derivatives also offer interesting possibilities for optical applications. A number of theoretical studies have predicted that a direct bandgap in the visible region would occur for sufficiently small graphene nanoribbons;[47,48] however, no observations of this finite size effect have been reported. Although a zero-gap semimetal, graphene may be oxidized in a manner that produces PL. In 2008, Dai and co-workers reported intrinsic luminescence from predominantly single-layer nanographene oxide (NGO) sheets in both the visible and NIR regions.[49] Activation and covalent grafting of hexabranched PEG stars onto the NGO surface resulted in significant darkening that was visible to the unaided eye, a phenomenon attributed to the opening of the epoxide groups

and ester hydrolysis, thereby leading to reduced local strain and concomitantly increased conjugation. Surprisingly, size-selected NGO-PEG fractions collected by density gradient ultracentrifugation yielded comparable optical and PL properties. The lack of apparent quantum confinement effects, which is in stark contrast to observations made with C-dots, suggests that the PL might originate from localized, conjugated aromatic domains within the NGO sheets. Nevertheless, by conjugating a B-cell-specific antibody to NGO-PEG, the authors showed the selective recognition and live imaging of Raji B-cells by using intrinsic NIR PL arising from the NGO. Interestingly, NGO was also exploited as a vehicle for the antibody-targeted delivery of the widely used chemotherapy drug doxorubicin, which was loaded onto the NGO surface by simple π-stacking-mediated physisorption.

Kikkawa and co-workers[50] reported broadband visible PL possessing a long NIR emission tail both for aqueous dispersions of GO and for solid GO samples drop-casted onto fused quartz. In this study, the authors observed that the progressive reduction of solid GO samples in a hydrazine vapor are coordinated with a marked red-shift in the PL band position, thus suggesting a gapping of the two-dimensional electronic system by removal of π electrons. After considering possible theoretical frameworks for interpreting these data, the authors proposed the emergence of a plausible Kekulé pattern of bond distortions to account for the observed behavior. They further noted that the loss of quantum yield during chemical reduction suggested that some regions might remain heavily oxidized.

In a recent study, Gokus et al.[51] discovered the induction of pronounced PL within single-layer graphene (SLG) flakes treated by an oxygen/argon (1:2) plasma. Confocal PL maps reveal bright, pointlike PL features for short treatment times (1–3 s), whereas for slightly longer exposures (5–6 s) spatially uniform broadband visible PL was observed across SLG flakes. Remarkably, because oxygen plasma etching proceeds layer-by-layer, bi- and multilayer flakes remained nonluminescent (Figure 24), thus implying that emission from the topmost layer is quenched by subjacent untreated layers. Spectral hole burning experiments suggest that the observed large spectral width (ca. 0.5 eV) mainly reflects homogeneous broadening of a single emissive species, that is uniform across the oxidized SLG sheet. This is supported by the fact that the PL transients were nearly uniform across the complete spectrum, thereby indicating that spectral diffusion as a result of energy migration, which is typical for heterogeneously broadened systems, is absent.

In contrast to previous work, Chhowalla and co-workers have described blue PL from solution-processed GO thin films deposited from thoroughly exfoliated suspensions.[52] These researchers hypothesize that PL from these chemically derived GO films originates from the radiative recombination of electron-hole pairs, localized within small, isolated $sp^2$ carbon clusters (likely containing only a few aromatic rings), which act as luminescence centers, embedded within the carbon-oxygen $sp^3$ matrix. During the initial stages of reductive treatment with hydrazine vapor, the fraction of strongly localized $sp^2$ sites increases, thereby enhancing the PL intensity by an order of magnitude for slightly reduced
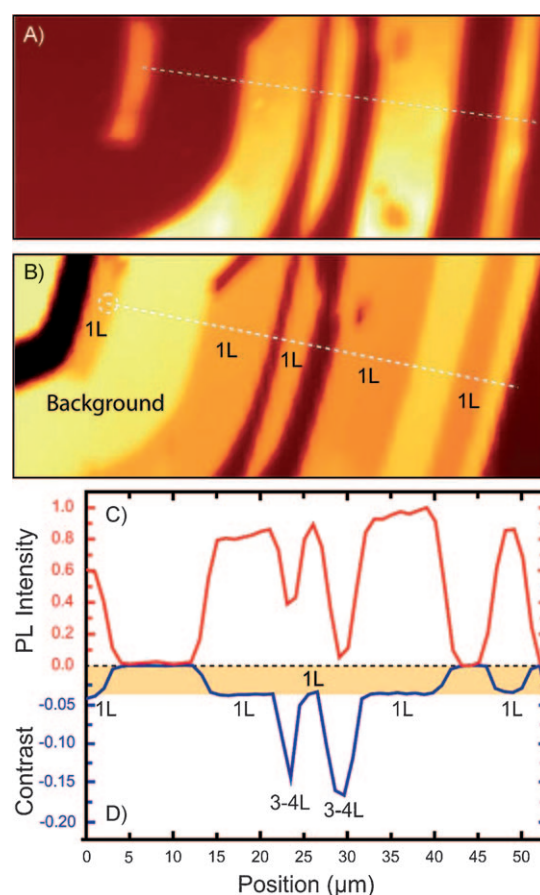


**Figure 24.** Correlation between PL and layer thickness. A) Confocal PL image; B) elastic scattering image of the same sample area. C,D) Corresponding cross-sections taken along the dashed lines in (A,B). PL is only observed from treated SLG (marked 1 L here). 3–4 L denotes a multilayer. Reproduced from Ref. [51] with permission.

GO thin films over as-deposited GO films. Interestingly, the trend is reversed at more advanced stages in the reduction process, which leads to eventual quenching of the PL signal. The subsequent PL quenching with longer reduction may be the result of percolation among these $sp^2$ configurations, thereby facilitating the transport of excitons to nonradiative recombination sites. It is notable that these scientists observed red and NIR emission comparable to that reported earlier[49,50] for GO films drop-casted from poorly dispersed suspensions.

Pan et al. have developed a simple hydrothermal route for cutting preoxidized micrometer-sized rippled graphene sheets into ultrafine graphene quantum dots (GQDs) with diameters mainly distributed in the 5–13 nm range.[53] These functionalized GQDs were found to exhibit bright blue PL (quantum yield ca. 7%), which has never been previously observed among the GQDs because of their large lateral dimensions. Following the hydrothermal deoxygenation process, more than 85% of the GQDs were found to consist of 1–3 layers and, intriguingly, the resulting GQDs showed $\lambda_{ex}$-dependent PL behavior, a feature broadly shared by the C-dots. The authors suggested that the blue PL may originate from free zigzag sites with a carbene-like triplet ground state. This

notion is consistent with the observed pH-switchable PL, during which the GQDs emit strongly under alkaline conditions but are almost completely quenched in acidic media.

In all of the examples cited in this Section, graphene materials were produced either by micromechanical cleavage or exfoliation of graphite by following a modified Hummers method. In an intriguing departure from these approaches, Giannelis and co-workers prepared a layered carbonaceous material containing both heteroatoms and fixed ammonium groups simply by pyrolysis of the molecular precursor bis(2-chloroethyl)amine hydrochloride at 260°C in open air.[54] Although the exact structure remains an open question, this material can essentially be regarded as a carbonaceous analogue of conventional layered inorganic materials such as smectic clays or layered double hydroxides. These layered carbons behave similarly to laponite, a well-known phyllomorphic aluminosilicate, are colloidally stable in water, possesses ion-exchange properties, and share many characteristics of GO. Indeed, the layered carbons present PL behavior quite similar to that observed in C-dots, including $\lambda_{ex}$-dependent emission spectra and a high quantum yield of 11%.

As remains the case for C-dots, the detailed mechanism and chemical species responsible for PL in graphene derivatives awaits further understanding. Throughout these studies, some interesting questions arise such as whether energy relaxation and spectral diffusion in GO-type materials are altered by aggregation and interlayer coupling and whether significant inhomogeneity of the oxidation profile exists within the GO plane. It also becomes apparent that while absolute values for the emissive quantum yields and an appreciation for inner filter effects will illuminate these questions, the accurate measurement of these quantities is problematic for ensembles of heterogeneous nanomaterials. These facts notwithstanding, taken together, the early results cited here suggest that GO may become a promising platform that paves the way toward interesting biomedical labeling and optoelectronics applications. An outstanding challenge in this regard is the ability to engineer desired molecular sp$^2$ topologies while controlling their organization and fraction in graphene. Advances along these lines are a near-certainty in the not-too-distant future.

## 6. Summary and Outlook

C-dots are interesting newcomers to the world of nanomaterials and are fascinating luminescent materials as well as promising building blocks for future nanodevices. Developing better synthetic routes and more detailed fundamental studies of their properties have a level of urgency, as there remains a good deal of room for improvement. Despite the fact that a full understanding of their photophysical properties has yet to emerge, they are indeed interesting nanomaterials in their own right. C-dots stand to have a huge impact in both health and environmental applications because of their potential to serve as nontoxic replacements to traditional heavy-metal-based QDs. Additionally, they can be made from a wide variety of synthetic techniques, including methods that employ inexpensive renewable resources such as lignocellulosic biomass wastes (for example, corn stover, switchgrass, used cooking oil) as starting materials.

Not surprisingly, given their low cost, ready scalability, excellent chemical stability, biocompatibility/nontoxicity, colloidal stability, and resilience of PL in vivo, C-dots have shown primary potential in optical imaging and related biomedical applications. In this regard, they share some of the attractive traits of groups of uniform materials based on organic salts (GUMBOS)[55,56] and fluorescent thiolate-capped gold nanoclusters[57] as prospective alternatives to Q-dots labels in biologically motivated experiments. However, the recent report demonstrating the capacity for photo-induced electron-transfer behavior in C-dots[14] means they may additionally hold compelling potential in battery technology as well as in photovoltaic devices, possibly as potential light-harvesting units. Additionally, the ability to easily introduce versatile functionality at the C-dot surface by rational conjugation chemistry allows them to be fine-tuned in ways beyond influencing optoelectronic properties, including the modulation of solubility in desired solvent systems and the suitability for coupling with various surfaces (bulk, nanoscale, or biological). By suitable doping, chemical manipulation, or as essential components of nanocomposites, they may open the door to a host of unforeseen applications ranging from contrast agents for magnetic resonance imaging (MRI) and magnetic data storage applications to battery electrodes. Ultimately, once a deeper understanding of their fundamental properties is achieved, one can even envision C-dot-based systems in organic light-emitting diodes (OLEDs), separation membranes, displays and backlights, drug delivery, and advanced cancer/photodynamic therapy. Only time will tell, but the future of these emergent nanolights positively appears bright.

[1] X. Y. Xu, R. Ray, Y. L. Gu, H. J. Ploehn, L. Gearheart, K. Raker, W. A. Scrivens, *J. Am. Chem. Soc.* **2004**, *126*, 12736–12737.

[2] A. B. Bourlinos, A. Stassinopoulos, D. Anglos, R. Zboril, V. Georgakilas, E. P. Giannelis, *Chem. Mater.* **2008**, *20*, 4539–4541.

[3] A. B. Bourlinos, A. Stassinopoulos, D. Anglos, R. Zboril, M. Karakassides, E. P. Giannelis, *Small* **2008**, *4*, 455–458.

[4] L. Cao, X. Wang, M. J. Meziani, F. S. Lu, H. F. Wang, P. J. G. Luo, Y. Lin, B. A. Harruff, L. M. Veca, D. Murray, S. Y. Xie, Y. P. Sun, *J. Am. Chem. Soc.* **2007**, *129*, 11318–11319.

[5] S. L. Hu, P. K. Bai, S. R. Cao, J. Sun, *Chem. J. Chin. Univ. Chin.* **2009**, *30*, 1497–1500.

[6] S. L. Hu, K. Y. Niu, J. Sun, J. Yang, N. Q. Zhao, X. W. Du, *J. Mater. Chem.* **2009**, *19*, 484–488.

[7] H. P. Liu, T. Ye, C. D. Mao, *Angew. Chem.* **2007**, *119*, 6593–6595; *Angew. Chem. Int. Ed.* **2007**, *46*, 6473–6475.

[8] J. Lu, J.-X. Yang, J. Wang, A. Lim, S. Wang, K. P. Loh, *ACS Nano* **2009**, *3*, 2367–2375.

[9] R. L. Liu, D. Q. Wu, S. H. Liu, K. Koynov, W. Knoll, Q. Li, *Angew. Chem.* **2009**, *121*, 4668–4671; *Angew. Chem. Int. Ed.* **2009**, *48*, 4598–4601.

[10] S. C. Ray, A. Saha, N. R. Jana, R. Sarkar, *J. Phys. Chem. C* **2009**, *113*, 18546–18551.

[11] Y. P. Sun, X. Wang, F. S. Lu, L. Cao, M. J. Meziani, P. J. G. Luo, L. R. Gu, L. M. Veca, *J. Phys. Chem. C* **2008**, *112*, 18295–18298.

[12] Y. P. Sun, B. Zhou, Y. Lin, W. Wang, K. A. S. Fernando, P. Pathak, M. J. Meziani, B. A. Harruff, X. Wang, H. F. Wang, P. J. G. Luo, H. Yang, M. E. Kose, B. L. Chen, L. M. Veca, S. Y. Xie, *J. Am. Chem. Soc.* **2006**, *128*, 7756–7757.

[13] L. Tian, D. Ghosh, W. Chen, S. Pradhan, X. Chang, S. Chen, *Chem. Mater.* **2009**, *21*, 2803–2809.

[14] X. Wang, L. Cao, F. S. Lu, M. J. Meziani, H. Li, G. Qi, B. Zhou, B. A. Harruff, F. Kermarrec, Y. P. Sun, *Chem. Commun.* **2009**, 3774–3776.

[15] S. T. Yang, L. Cao, P. G. Luo, F. S. Lu, X. Wang, H. F. Wang, M. J. Meziani, Y. F. Liu, G. Qi, Y. P. Sun, *J. Am. Chem. Soc.* **2009**, *131*, 11308–11309.

[16] S.-T. Yang, X. Wang, H. Wang, F. Lu, P. G. Luo, L. Cao, M. J. Meziani, J.-H. Liu, Y. Liu, M. Chen, Y. Huang, Y.-P. Sun, *J. Phys. Chem. C* **2009**, *113*, 18110–18114.

[17] Q. L. Zhao, Z. L. Zhang, B. H. Huang, J. Peng, M. Zhang, D. W. Pang, *Chem. Commun.* **2008**, 5116–5118.

[18] L. Y. Zheng, Y. W. Chi, Y. Q. Dong, J. P. Lin, B. B. Wang, *J. Am. Chem. Soc.* **2009**, *131*, 4564–4565.

[19] J. G. Zhou, C. Booker, R. Y. Li, X. T. Zhou, T. K. Sham, X. L. Sun, Z. F. Ding, *J. Am. Chem. Soc.* **2007**, *129*, 744–745.

[20] H. Zhu, X. L. Wang, Y. L. Li, Z. J. Wang, F. Yang, X. R. Yang, *Chem. Commun.* **2009**, 5118–5120.

[21] M. Bottini, T. Mustelin, *Nat. Nanotechnol.* **2007**, *2*, 599–600.

[22] J. Evans, *Chem. World* **2006**, *3*, 18–18.

[23] H. Peng, J. Travas-Sejdic, *Chem. Mater.* **2009**, *21*, 5563–5565.

[24] S. Empedocles, M. Bawendi, *Acc. Chem. Res.* **1999**, *32*, 389–396.

[25] T. Trindade, P. O'Brien, N. L. Pickett, *Chem. Mater.* **2001**, *13*, 3843–3858.

[26] A. D. Yoffe, *Adv. Phys.* **2001**, *50*, 1–208.

[27] S. Schuppler, S. L. Friedman, M. A. Marcus, D. L. Adler, Y. H. Xie, F. M. Ross, Y. J. Chabal, T. D. Harris, L. E. Brus, W. L. Brown, E. E. Chaban, P. F. Szajowski, S. B. Christman, P. H. Citrin, *Phys. Rev. B* **1995**, *52*, 4910–4925.

[28] S. Schuppler, S. L. Friedman, M. A. Marcus, D. L. Adler, Y. H. Xie, F. M. Ross, T. D. Harris, W. L. Brown, Y. J. Chabal, L. E. Brus, P. H. Citrin, *Phys. Rev. Lett.* **1994**, *72*, 2648–2651.

[29] W. L. Wilson, P. F. Szajowski, L. E. Brus, *Science* **1993**, *262*, 1242–1244.

[30] S.-J. Yu, M.-W. Kang, H.-C. Chang, K.-M. Chen, Y.-C. Yu, *J. Am. Chem. Soc.* **2005**, *127*, 17604–17605.

[31] A. Krueger, *Adv. Mater.* **2008**, *20*, 2445–2449.

[32] A. Krueger, *J. Mater. Chem.* **2008**, *18*, 1485–1492.

[33] A. Krueger, *Chem. Eur. J.* **2008**, *14*, 1382–1390.

[34] G. A. Baker, S. N. Baker, S. Pandey, F. V. Bright, *Analyst* **2005**, *130*, 800–808.

[35] J. R. Lakowicz, *Principles of Fluorescence Spectroscopy*, 3rd ed., Springer, New York, **2006**.

[36] S. C. Pu, M. J. Yang, C. C. Hsu, C. W. Lai, C. C. Hsieh, S. H. Lin, Y. M. Cheng, P. T. Chou, *Small* **2006**, *2*, 1308–1313.

[37] D. R. Larson, W. R. Zipfel, R. M. Williams, S. W. Clark, M. P. Bruchez, F. W. Wise, W. W. Webb, *Science* **2003**, *300*, 1434–1436.

[38] H. L. Qi, Y. Peng, Q. Gao, C. X. Zhang, *Sensors* **2009**, *9*, 674–695.

[39] L. H. Zhang, X. Q. Zou, E. Ying, S. J. Dong, *J. Phys. Chem. C* **2008**, *112*, 4451–4454.

[40] Y. Bae, N. Myung, A. J. Bard, *Nano Lett.* **2004**, *4*, 1153–1161.

[41] N. Myung, Y. Bae, A. J. Bard, *Nano Lett.* **2003**, *3*, 1053–1055.

[42] Z. F. Ding, B. M. Quinn, S. K. Haram, L. E. Pell, B. A. Korgel, A. J. Bard, *Science* **2002**, *296*, 1293–1297.

[43] X. H. Gao, L. L. Yang, J. A. Petros, F. F. Marshal, J. W. Simons, S. M. Nie, *Curr. Opin. Biotechnol.* **2005**, *16*, 63–72.

[44] R. Hardman, *Environ. Health Perspect.* **2006**, *114*, 165–172.

[45] J. K. Jaiswal, S. M. Simon, *Trends Cell Biol.* **2004**, *14*, 497–504.

[46] S. D. Li, L. Huang in *7th International Symposium on Polymer Therapeutics*, Valencia, Spain, American Chemical Society, **2007**, pp. 496–504.

[47] Y. W. Son, M. L. Cohen, S. G. Louie, *Nature* **2006**, *444*, 347–349.

[48] K. Kusakabe, M. Maruyama, *Phys. Rev. B* **2003**, *67*, 092406.

[49] X. Sun, Z. Liu, K. Welsher, J. Robinson, A. Goodwin, S. Zaric, H. Dai, *Nano Res.* **2008**, *1*, 203–212.

[50] Z. T. Luo, P. M. Vora, E. J. Mele, A. T. C. Johnson, J. M. Kikkawa, *Appl. Phys. Lett.* **2009**, *94*, 111909.

[51] T. Gokus, R. R. Nair, A. Bonetti, M. Bohmler, A. Lombardo, K. S. Novoselov, A. K. Geim, A. C. Ferrari, A. Hartschuh, *ACS Nano* **2009**, *3*, 3963–3968.

[52] G. Eda, Y.-Y. Lin, C. Mattevi, H. Yamaguchi, H.-A. Chen, I.-S. Chen, C.-W. Chen, M. Chhowalla, *Adv. Mater.* **2010**, *22*, 505–509.

[53] D. Pan, J. Zhang, Z. Li, M. Wu, *Adv. Mater.* **2010**, *22*, 734–738.

[54] A. B. Bourlinos, V. Georgakilas, R. Zboril, A. Bakandritsos, A. Stassinopoulos, D. Anglos, E. P. Giannelis, *Carbon* **2009**, *47*, 519–526.

[55] D. K. Bwambok, B. El-Zahab, S. K. Challa, M. Li, L. Chandler, G. A. Baker, I. M. Warner, *ACS Nano* **2009**, *3*, 3854–3860.

[56] A. Tesfai, B. El-Zahab, D. K. Bwambok, G. A. Baker, S. O. Fakayode, M. Lowry, I. M. Warner, *Nano Lett.* **2008**, *8*, 897–901.

[57] C. A. J. Lin, T. Y. Yang, C. H. Lee, S. H. Huang, R. A. Sperling, M. Zanella, J. K. Li, J. L. Shen, H. H. Wang, H. I. Yeh, W. J. Parak, W. H. Chang, *ACS Nano* **2009**, *3*, 395–401.